energies

Article

Post-Disaster Power Outage Risk Perception of Medium- and Low-Voltage Distribution Networks Under Typhoons Based on Graded Building Damage: Integrating Dempster–Shafer Theory, Parallel Deep Learning and Multi-Source Data Fusion

Yu Zou [1], Juan Bai [2], Xiaonan Shen [2], Yang Luo [3], Yiran Mo [4], Xingtong Xie [1], Honghui Zhang [5,*], Mingzhi Bin [3], Yongtu Li [6], Pingping Gong [6] and Linfei Yin [6]

1 Production Engineering Department, Guangxi Power Grid Co., Ltd. Qinzhou Power Supply Bureau, Qinzhou 535000, China; zou_y.qzg@gx.csg.cn (Y.Z.); 15977118006@163.com (X.X.)
2 Production Control Center, Guangxi Power Grid Co., Ltd. Qinzhou Power Supply Bureau, Qinzhou 535000, China; m13557776209@163.com (J.B.); shen_xn.qzg@gx.csg.cn (X.S.)
3 Camp Supply Command Center, Guangxi Power Grid Co., Ltd. Qinzhou Pubei Power Supply Bureau, Qinzhou 535000, China; m15907778118@163.com (Y.L.); 18321153387@163.com (M.B.)
4 Camp Supply Command Center, Guangxi Power Grid Co., Ltd. Qinzhou Lingshan Power Supply Bureau, Qinzhou 535000, China; 120191058@163.com
5 Qinzhou Lingshan Power Supply Bureau, Guangxi Power Grid Co., Ltd. Qinzhou Power Supply Bureau, Qinzhou 535000, China
6 School of Electrical Engineering, Guangxi University, Nanning 530004, China; liyongtu@st.gxu.edu.cn (Y.L.); gongpp@gxu.edu.cn (P.G.); yinlinfei@gxu.edu.cn (L.Y.)
* Correspondence: zhanghh0472@gx.csg.cn or zhanghh0472@im.gxqz.csg.cn

Abstract

The medium- and low-voltage distribution network is a critical hub connecting the transmission grid and end-users, and its power supply reliability directly determines livelihood security and socio-economic operational efficiency. Typhoon-induced strong winds and rainfall often trigger large-scale power outage risks, severely threatening power grid security and resilience. To achieve the rapid and accurate perception of outage risk areas based on building damage after typhoons, this study proposes the ResiDS-Net method, which infers distribution network outage risk levels by identifying building damage levels. An improved Dempster–Shafer evidence theory is here adopted to fuse the outputs of CM-ResNet50, Inception-V3 and DenseNet121, enhancing perception accuracy. A two-stage "coarse screening–fine judgment" framework using dual datasets is established to quickly identify large-scale suspected power outage areas from building group damage data. To address the issue that equating building damage with power outages reduces judgment accuracy, this study further develops a hierarchical building damage dataset, classifying individual buildings by damage level to achieve precise outage risk identification. Our experiments show that ResiDS-Net achieves 96.66% and 93.00% accuracy on the two datasets, 2.13% and 2.50% higher than nine comparative networks including Inception-V3. The proposed method effectively improves outage risk perception precision and provides a scientific basis for power emergency repair. It should be noted that the proposed method provides building-damage-based outage risk inference for emergency decision support, rather than the direct detection of verified actual outage status.

Keywords: typhoon disasters; distribution network power outages; ResiDS-Net; improved Dempster–Shafer evidence; CM-ResNet50; two-stage power outage risk perception method

Academic Editor: Bertrand Raison

Received: 8 June 2026
Revised: 10 July 2026
Accepted: 12 July 2026
Published: 14 July 2026

1. Introduction

As the critical link connecting energy production and end consumption in power systems, distribution networks are characterized by wide coverage, complex topology and outdoor-exposed equipment, whose operational reliability is directly related to the normal order of social production and daily life [1]. Extreme meteorological disasters such as typhoons are the primary risk source threatening the safety of distribution networks in coastal areas. Strong winds and heavy rainfall often cause pole and tower collapse and line breakage, leading to large-scale regional power outages [2]. In addition, the persistent heavy rainfall associated with typhoons can easily cause urban flooding. Power facilities located close to the ground—such as distribution transformers and ring main units—are prone to insulation failure and equipment malfunctions after being washed away or submerged by rainwater, which can also lead to widespread power outages [3]. However, existing post-disaster perception methods frequently suffer from high misjudgment rates and inadequate robustness in complex noisy environments. This research is therefore undertaken with the objective of developing a highly accurate and resilient power outage risk perception method that overcomes these limitations through advanced multi-model fusion and fine-grained damage assessment.

Current post-disaster power outage risk perception studies based on satellite remote sensing mostly adopt single-stage whole-image classification, which directly determines whether an area is experiencing a power outage through global image features [4]. However, single-stage whole-image classification system has two core bottlenecks. First, the inherent limitation of coarse-grained labels; existing datasets generally equate the presence of building damage in an area with the occurrence of a power outage, failing to distinguish between minor damage that does not affect power supply and severe damage that causes outages, resulting in a large number of misjudgments [5]. Second, the capability limitation of single models; a single convolutional neural network (CNN), constrained by its architectural characteristics, struggles to simultaneously capture large-scale spatial distribution features and local fine-grained damage features. Its perception accuracy and generalization ability degrade significantly in complex noisy scenarios, such as those with cloud occlusion and image fogging [6]. To address these issues, this study proposes a novel two-stage distribution network power outage risk perception method based on improved Dempster–Shafer evidence theory. Through the progressive architecture of "rapid large-scale coarse screening–individual building fine judgment" combined with multi-model decision fusion technology, it effectively overcomes the high misjudgment rate and insufficient robustness of traditional methods in complex scenarios.

Existing distribution network power outage risk perception methods are mainly divided into three categories, namely, centralized physical quantity detection, distributed collaborative detection and data-driven intelligent detection, each with its own applicable scenarios and limitations. The centralized detection method based on maximum likelihood estimation constructs a probabilistic model to identify power outages by collecting global node loads and branch power flow data. It boasts a mature theoretical system and high accuracy in small-scale networks with complete measurements, but faces significant communication bandwidth bottlenecks and single point of failure risks, and has extremely poor scalability in scenarios with sparse measurements in medium- and low-voltage distribution networks [7]. The distributed detection method based on a divide-and-conquer strategy completes parallel detection through subnet partitioning and limited neighborhood communication, which significantly reduces communication and computational costs and greatly improves scalability. However, its performance is highly dependent on reasonable subnet partitioning and node coordination mechanisms. Faults at subnet boundaries are prone to detection blind spots, and it is difficult to adapt to scenarios with dynamic topology changes in distribution networks [8]. Data-driven methods, such as change point detection combined with projected gradient descent, do not require reliance on accurate physical models of power grids. They can adapt to complex scenarios with unknown topological parameters and fit nonlinear fault characteristics, but are highly sensitive to measurement data quality, have high training and parameter update costs, and struggle to fully mine implicit fault information in high-dimensional data [9].

From the perspective of the disaster resilience enhancement of distribution networks, the existing research on outage estimation and remote sensing damage assessment can be further divided into two closely related branches, each with unsolved limitations that form the core research gap of this subject.

First, regarding distribution network outage estimation after extreme meteorological events, most existing studies construct probabilistic prediction models based on pre-disaster topological parameters, meteorological forecast data and historical fault statistics [10]. These methods deliver satisfactory performance in pre-disaster risk warning, but rely heavily on the integrity of grid operation data and topology information. Following severe typhoon disasters, on-site measurement equipment is frequently damaged and communication links are disrupted, making real-time operation data inaccessible and sharply reducing the practicability of such methods. In recent years, satellite remote sensing technology has provided a new data source independent of on-site communication conditions for post-disaster outage perception. Nevertheless, most current remote sensing-based outage perception studies remain limited to coarse-grained regional binary classification, which directly equates the presence of damaged buildings in a region with power outages, and thus yields a generally high false positive rate.

Second, regarding remote sensing-based infrastructure damage assessment in disaster scenarios, current research predominantly focuses on the damage classification of buildings or roads, which supports post-disaster loss statistics and relief resource allocation [11]. However, typhoon events are typically accompanied by persistent heavy cloud cover, rainfall-induced atmospheric haze and image blurring, which severely degrade the quality of post-disaster satellite remote sensing imagery. These interferences obscure the fine-grained features of building damage and raise the difficulty of accurate damage boundary identification, while existing single-network damage classification models generally suffer from notable performance degradation under such noisy conditions and lack targeted robustness design for typhoon-affected remote sensing scenarios.

In recent years, with the rapid development of artificial intelligence, convolutional neural networks have received extensive attention from researchers due to their powerful fine-grained feature discrimination capability, and have been widely applied in industrial and medical detection fields. The diagnostically fine-tuned ResNet50 achieved a classification accuracy of 98.77% on the public lung cancer dataset [12]. Inception-V3 reached 96.88% accuracy in mineral image classification tasks [13]. DenseNet121 with Block-End feature enhancement attained 99.25% benign–malignant classification accuracy on the public breast cancer histopathology dataset BreakHis 40X [14]. The DS-PSO hybrid attack detection method, which integrates Dempster–Shafer evidence theory and Particle Swarm Optimization (PSO), effectively solves the problems of low detection accuracy and high false positive rate faced by traditional single-model attack detection methods in hybrid interest flooding attack scenarios in Vehicular Named Data Networking (VNDN), which are caused by designing only for single attack types and lacking effective multi-feature fusion [15]. The Unified Resilience Model (URM) with CNN-LSTM deep learning attained 12.42% performance factor improvement and 10.99% resilience factor enhancement on the Western Interconnection synthetic power grid dataset under variable battery capacity conditions [16]. These cross-domain studies verify the effectiveness of CNN models in fine-grained image classification and DS evidence theory in multi-source decision fusion, providing a technical reference for the method design in this study. Leveraging the complementary strengths of these powerful feature extractors and overcoming the limitations of isolated single-model decisions, this study proposes a novel ResiDS-Net network that combines CM-ResNet50, Inception-V3, DenseNet121 and the improved Dempster–Shafer (DS) evidence theory. It performs fused decision-making on the judgments of multiple networks through the improved DS evidence theory to achieve the accurate perception of power outage risk areas in distribution networks, as compared with other methods (shown in Table 1). The main contributions of this study are summarized as follows:

1. Aiming at the first research gap, related to the fact that it is difficult to balance large-scale perception speed and fine-grained judgment accuracy, this study constructs a two-stage "coarse screening-fine judgment" perception framework with dual datasets. The first stage realizes the rapid delineation of large-scale suspected outage areas based on building group damage data, and the second stage completes an accurate outage risk assessment through individual building damage grading, which breaks through the limitation of traditional single-stage coarse-grained classification;
2. Most mainstream traditional deep learning networks adopt a serial architecture. Although the learning capability of the network is enhanced as the number of layers increases, a degradation problem occurs when the layer count reaches a certain threshold [17]. As the depth of serial networks continues to grow, part of the important feature information is lost during inter-layer information transmission, and the training time is also prolonged. A major novelty of this work is the introduction of a parallel architecture in ResiDS-Net, which can extract important multi-scale feature information through three sub-networks and reduce the loss of critical feature information;
3. Aiming at the second research gap, related to the fact that a single model has an insufficient feature extraction ability for noisy remote sensing images, the proposed ResiDS-Net in this study fuses the noise-resistant deep feature extraction capability of CM-ResNet50, the multi-scale feature capture capability of Inception-V3, and the fine-grained feature reuse capability of DenseNet121 via the improved Dempster–Shafer evidence theory, thereby improving the prediction accuracy of power outage risk areas;
4. Aiming at the defects of traditional Dempster–Shafer (DS) evidence theory in multi-source decision fusion, including the fact that basic belief assignments (BBAs) are susceptible to noise interference, evidence weights are equalized, and conflicting evidence leads to decision paradoxes, the improved DS method proposed in this study introduces an error correction term to realize the normalization of belief assignments, adaptively assigns evidence weights based on similarity and support degree, optimizes the conflict fusion rule and adds a decision probability conversion step, which can help it to adapt to the characteristics of multi-source heterogeneous data in distribution networks;
5. Compared with ResNet50, this study proposes a Conv Modulation convolutional modulation module and integrates it into CM-ResNet50. By stabilizing feature distribution through layer normalization, capturing global contextual information via large-kernel depthwise convolution, and combining GELU nonlinear activation with a dual-branch element-wise feature self-modulation mechanism, it enhances the convolutional network's ability to focus on deep damage features and robustness to noise in remote sensing images, and addresses the inherent limitations of ResNet50, namely, its sensitivity to cloud cover and fog interference and the insufficient representation of fine-grained damage features. Overall, ResiDS-Net substantially reduces the misjudg-

ment rate in power outage risk perception and delivers markedly superior robustness in challenging post-disaster scenarios compared with existing approaches.

Table 1. Comparison of power outage risk perception methods for medium- and low-voltage distribution networks.

Name	Type	Advantages	Disadvantages
Centralized detection method based on maximum likelihood estimation	Centralized detection method	Mature theoretical system; high accuracy in small-scale networks	Significant communication bottleneck; poor scalability
Parallel and distributed detection method based on divide-and-conquer strategy	Distributed detection method	High scalability; low communication cost	Accuracy depends on reasonable partitioning and coordination mechanisms
Change point detection method combined with projected gradient descent	Data-driven detection method	Capable of fitting complex features; adaptable to unknown power outage scenarios in distribution networks	High parameter learning cost; sensitive to data quality
The proposed ResiDS-Net detection method	Data-driven deep learning detection method	Strong capability in fitting complex features; capable of handling conflicting multi-source data; applicable to unknown power outage scenarios in complex backgrounds	Complex network structure; dependent on data quality

The organization of this paper is as follows: Section 2 introduces the dataset for power outage risk perception based on building group damage and the dataset for power outage risk perception based on hierarchical building damage after typhoon disasters. Section 3 elaborates the proposed ResiDS-Net method for power outage risk perception in medium- and low-voltage distribution networks. Section 4 presents the ten network models employed in the two post-typhoon power outage risk perception datasets. Section 5 concludes the whole paper.

2. Composition and Analysis of the Power Outage Risk Perception Dataset Based on Building Group Damage After Typhoon Disasters

This section introduces the employed power outage risk perception dataset based on building group damage after typhoon disasters and the power outage risk perception dataset based on graded building damage.

2.1. Composition and Analysis of the Power Outage Risk Perception Dataset Based on Building Group Damage After Typhoon Disasters

The power outage risk perception dataset for building damage under typhoon disasters constructed in this study is derived from the internationally authoritative XBD (Extended Building Damage) satellite remote sensing benchmark dataset. As the official core dataset of the xView2 Global Disaster Remote Sensing Challenge, XBD is one of the largest and most well-annotated public datasets in the field of disaster building damage recognition. It contains high-resolution pre- and post-disaster satellite images covering various natural disasters worldwide and corresponding building-level damage annotations, with the aim of promoting the development of intelligent analysis technologies for disaster remote sensing images. According to the official definition of the World Meteorological

Organization (WMO), typhoons and hurricanes are essentially the same meteorological phenomenon. They share identical formation mechanisms and damage patterns, and are merely different names for the same type of weather system in different ocean basins. Targeting the specific requirements of distribution network power outage risk perception under typhoon disasters, this study selects post-disaster remote sensing image data of four typical severe hurricane events from the XBD dataset, namely, Harvey (2017), Matthew (2016), Florence (2018) and Michael (2018). These four events correspond to four representative damage modes, namely, flood immersion damage, localized strong wind damage, combined storm surge and rainstorm damage, and complete structural damage caused by strong winds. They cover most damage types that typhoon disasters may cause in coastal areas, and have good scene diversity and geographical representativeness [18]. For terminological consistency across the full manuscript, these four events are uniformly referred to as typhoon disasters in this study.

During the dataset construction process, this study first performs unified preprocessing on the original images. A regional binary labeling strategy is adopted to construct power outage risk perception labels, as follows: if there is at least one damaged building in an image, the image is labeled as a suspected outage area; if all buildings in the slice are intact, it is labeled as a normal area. This labeling method is logically consistent with traditional power outage risk perception methods based on the entire image, and can simulate the practical application scenario of quickly delineating suspected power outage areas through large-scale remote sensing images immediately after a disaster occurs. This dataset can effectively verify the model's ability to rapidly identify suspected power outage areas in large-scale regions, and provides reliable data support for the coarse screening stage of the two-stage "coarse screening–fine judgment" perception framework. The composition of the training, validation, and test sets in this dataset is shown in Table 2.

Table 2. Composition of the training, validation, and test sets.

Name	Harvey	Matthew	Florence	Michael
Training set	619	461	625	677
Validation set	188	183	230	216
Test set	207	140	211	191

To explicitly illustrate the data composition and ensure experimental reproducibility, the detailed class distribution of this binary dataset is presented in Table 3, which summarizes the sample counts of the two categories—no damage (normal power supply area) and building damage (suspected outage area)—across the training, validation, and test sets.

Table 3. Composition of the training, validation, and test sets.

Category	Training Set	Validation Set	Test Set
No damage (normal power supply area)	1456	504	464
Building damage (suspected outage area)	926	313	285
Total	2382	817	749

2.2. Composition and Analysis of the Power Outage Risk Perception Dataset Based on Graded Building Damage After Typhoon Disasters

To address the inherent limitations of the power outage risk perception dataset based on building damage after typhoon disasters—its inability to distinguish minor building damage that does not affect power supply from severe structural damage that causes power interruption, and its direct equivalence between the presence of damaged buildings in a region and power outages in the distribution network—this study further constructs the

Power Outage Risk Perception Dataset Based on Graded Building Damage After Typhoon Disasters. Through fine-grained damage annotations at the individual building level, it establishes a quantitative mapping relationship between different damage degrees and estimated power outage probabilities, providing data support for the precise correction stage of the two-stage power outage risk perception framework. This dataset is also constructed based on the XBD benchmark dataset, with exactly the same data sources as the first dataset. Both select pre- and post-disaster satellite images of the four typical severe typhoon events (Harvey, Matthew, Florence and Michael), ensuring the consistency and comparability of the two datasets in terms of disaster scenarios, image quality and geographical distribution.

Different from the regional binary classification labeling adopted in the first dataset, this dataset adopts a four-category labeling system at the individual building level. Strictly following the official damage grading standard of the XBD Challenge, building damage levels are divided into four mutually exclusive and progressive grades, as follows: no damage, indicating that the building structure is intact with a corresponding power outage risk probability of 0; minor damage, referring to non-structural damage to the building with a corresponding power outage risk probability of 0; major damage, meaning structural damage to the building with a corresponding high power outage risk probability; and destruction, representing the complete collapse of the building with a corresponding power outage risk probability of 1. This mapping relationship is based on the strong spatial coupling characteristics between medium- and low-voltage distribution networks and buildings; lines and poles of medium- and low-voltage distribution networks are mostly laid along roads and around buildings, usually with a spatial distance of less than 50 m from buildings. The damage degree of buildings directly reflects the intensity of typhoon destructive force in the area, thereby characterizing the damage state of surrounding power facilities. In the dataset construction process, this study first accurately segments and extracts all independent individual building images from the original large-format satellite images based on the building vector boundaries provided by XBD, and uniformly crops them to a standard size of 224×224 pixels. Then, the damage grade of each building is manually reviewed and calibrated, and invalid samples with fuzzy labels and unclear boundaries are eliminated. For borderline samples that are difficult to grade, the judgment strictly follows the official annotation specification of the xView2 challenge; all disputed cases are jointly discussed and determined by two annotators with remote sensing interpretation experience, so as to ensure annotation consistency. Formal inter-annotator agreement metrics were not calculated in this study. Finally, the dataset is randomly divided into training, validation, and test sets at a ratio of 7:1:2.

Compared with the first dataset, this dataset achieves an annotation upgrade from regional coarse-grained to individual building fine-grained levels, enabling the accurate quantification of the proportion and distribution of buildings with different damage degrees within a region. For regions marked as suspected power outage areas in the first-stage coarse screening, this study conducts a secondary judgment by counting whether there are severely damaged or completely destroyed buildings in the region, with the following logic: if only undamaged or slightly damaged buildings exist, the region is identified as having minor damage but normal power supply and is excluded; a region is finally identified as a high-outage-risk area only when buildings with major damage or destruction grades are present. The two datasets form a complementary verification system of "large-scale rapid delineation–fine-grained precise correction", providing a comprehensive and reliable data foundation for the training and performance evaluation of the ResiDS-Net model. The composition of the training, validation, and test sets in this dataset is shown in Table 4.

Table 4. Composition of the training, validation, and test sets.

Name	Harvey	Matthew	Florence	Michael
Training set	969	245	276	300
Validation set	240	100	360	130
Test set	110	90	110	90

To explicitly illustrate the data composition of the fine-grained grading task and ensure experimental reproducibility, the detailed class distribution of the four damage grades in the graded building damage dataset is presented in Table 5, which summarizes the sample counts of No Damage, Minor Damage, Major Damage, and Destruction across the training, validation, and test subsets.

Table 5. Class distribution of the graded building damage four-class classification dataset.

Category	Training Set	Validation Set	Test Set
No damage	700	100	200
Minor Damage	700	100	200
Major Damage	700	100	200
Destruction	690	100	200
Total	2790	400	800

Based on the above dataset construction and labeling rules, three core terms throughout the two-stage perception framework are uniformly defined for clarity and terminological consistency:

Power outage risk perception—This refers to the task of indirectly inferring the power interruption probability of medium- and low-voltage distribution networks using building damage grade features extracted from satellite remote sensing images. As a risk screening approach based on proxy indicators, it outputs graded outage risk probability rather than ground-truth-verified actual outage states, and is positioned to provide auxiliary decision support for post-disaster emergency responses.

Suspected outage area—This corresponds to the output of the first-stage coarse screening and the labeling result of the first dataset. It refers to the regional scope preliminarily judged to have outage potential according to the overall damage state of building groups, aiming to rapidly narrow down the investigation range from large-scale disaster-affected areas, and it may contain a certain proportion of false alarms.

Final identified high outage risk area—This corresponds to the output of the second-stage fine judgment and the grading result of the second dataset. On the basis of the suspected outage area, regions containing buildings with major damage or destruction grade after fine-grained individual building damage verification are classified into this category. They are judged to have a high probability of distribution network failure and serve as the final output of the two-stage perception framework.

3. ResiDS-Net Based Power Outage Risk Perception Method for Medium- and Low-Voltage Distribution Networks

This study proposes the ResiDS-Net based power outage risk perception method for medium- and low-voltage distribution networks. By fusing the anti-noise deep feature extraction capability of CM-ResNet50, the multi-scale feature capture capability of Inception-V3, and the fine-grained feature reuse capability of DenseNet121 through the improved DS evidence theory, it can adapt to the multi-source heterogeneous data characteristics of distribution networks and improve the accuracy of power outage risk perception.

3.1. CM-ResNet50 of the Proposed ResiDS-Net Based Power Outage Risk Perception Method for Medium- and Low-Voltage Distribution Networks

The CM-ResNet50 proposed in this study takes ResNet50 as the backbone network. ResNet50 consists of a Stem layer and four feature stages. The Stem layer contains a 7×7 convolution and a max pooling layer, and the four feature stages are sequentially named layer1 to layer4. Each feature stage includes multiple Bottleneck Blocks, which implement deep feature extraction through residual connections, convolution layers, BatchNorm and ReLU activation functions. This effectively solves the vanishing gradient problem and endows both a strong feature representation capability and training stability [19].

To address the problems whereby the original ResNet50 is sensitive to noise interference in remote sensing images such as cloud cover and fog in typhoon disaster building damage detection, and its single convolution structure struggles to capture global contextual information and fine-grained damage features simultaneously, CM-ResNet50 introduces a Conv Modulation convolution modulation module after layer4 of feature extraction and before global average pooling. The Conv Modulation module first stabilizes the deep feature distribution through LayerNorm to suppress noise, then uses large-kernel depthwise convolution with a kernel size of 11 to capture large-scale global contextual information, and combines this with the GELU nonlinear activation function to enhance the flexibility of feature representation. Finally, it realizes adaptive focusing on key damage features through a dual-branch feature element-wise self-modulation mechanism, wherein the attention branch and the value branch perform element-wise multiplication. A residual connection is designed inside the Conv Modulation module to add the original input features and the modulated features element-wise. This ensures that while strengthening key damage features, the original deep semantic information extracted by the ResNet50 backbone will not be lost. It enhances the convolutional network's ability to focus on deep damage features and its robustness to remote sensing image noise, and can address the shortcomings of ResNet50, in terms of its sensitivity to cloud and fog interference and the insufficient expression of fine-grained damage features. The structure of the Conv Modulation module is shown in Figure 1, and the network structure of CM-ResNet50 is shown in Figure 2. In Figure 1, $\circledast$ denotes element-wise multiplication and $\oplus$ denotes feature-wise addition.

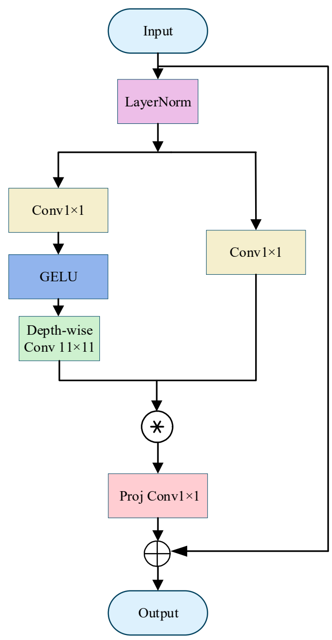

Figure 1. Structure of the proposed Conv Modulation module.

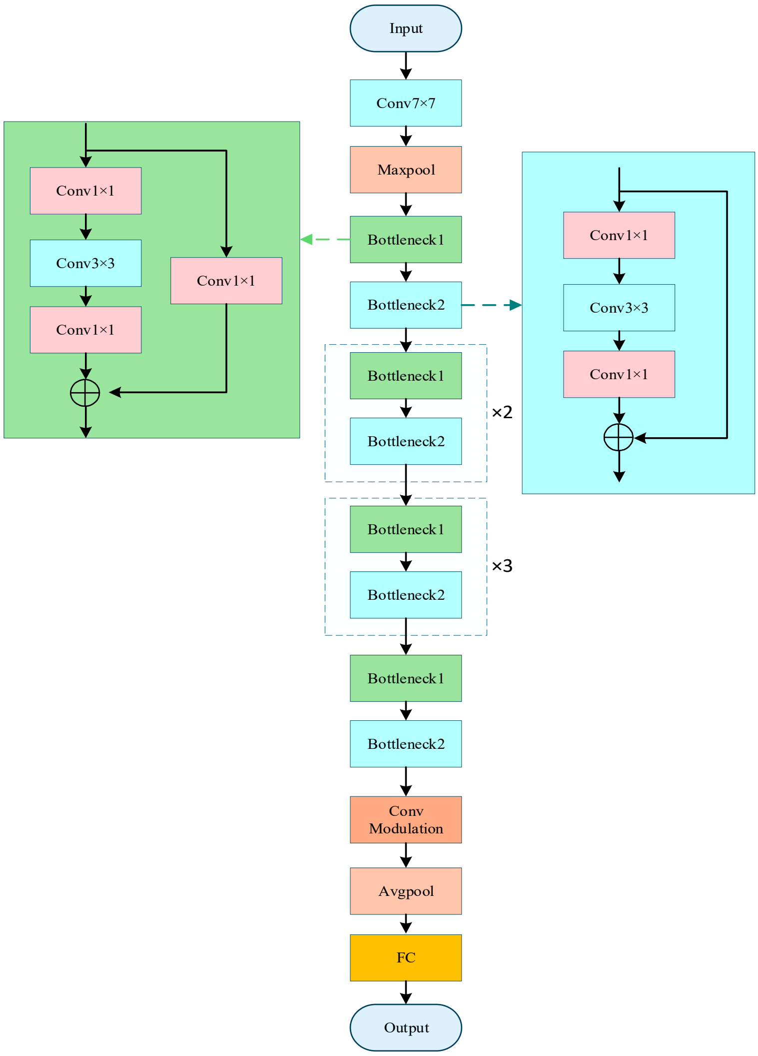

Figure 2. Structure of the proposed CM-ResNet50.

Let the input of the Conv Modulation module be the feature map $X \in \mathrm{R}^{B\times C\times H\times W}$ output by the fourth feature stage of ResNet50, where B is the batch size, C is the number of channels, and H and W are the height and width of the feature map, respectively. The computational flow of the Conv Modulation module is as follows:

$$X_{\mathrm{norm}} = \mathrm{LN}(X) \tag{1}$$

Herein, $\mathrm{LN}(\cdot)$ denotes the channel-first Layer Normalization operation, which computes the mean and variance along the spatial dimensions for each channel of each sample, and then performs the normalization transformation.

Subsequently, the normalized feature is fed into two parallel branches to generate the attention feature map and the value feature map, respectively. The attention branch undergoes a 1×1 pointwise convolution, GELU nonlinear activation, and 11×11 depthwise convolution to capture large-scale global contextual information, as shown in Equation (2).

$$A = \mathrm{Conv}_{11\times 11,\mathrm{depth}}(\mathrm{GELU}(\mathrm{Conv}_{1\times 1}(X_{\mathrm{norm}}))) \tag{2}$$

Herein, $\mathrm{Conv}_{1\times 1}(\cdot)$ denotes the 1×1 pointwise convolution, $\mathrm{GELU}(\cdot)$ is the Gaussian Error Linear Unit activation function, and $\mathrm{Conv}_{11\times 11,\mathrm{depth}}(\cdot)$ denotes the 11×11 depthwise convolution with the number of groups set equal to the number of channels, where each channel is convolved independently. The value branch generates the value feature map through a 1×1 pointwise convolution, and the calculation process is shown in Equation (3).

$$V = \mathrm{Conv}_{1\times1}(X_{\mathrm{norm}}) \tag{3}$$

Subsequently, feature element-wise self-modulation is performed, where the attention feature map and the value feature map are multiplied element-wise to achieve the adaptive weighted enhancement of key damage features and the suppression of background noise features, as shown in Equation (4).

$$M = A \odot V \tag{4}$$

Herein, M is the modulated feature map, A is the attention feature map generated by the attention branch, V is the value feature map generated by the value branch, and $\odot$ denotes the element-wise multiplication operation.

Finally, a 1×1 projection convolution is performed on the modulated feature map to integrate feature information; then, the original input features and the modulated features are added element-wise through a residual connection to avoid information loss in deep networks, as shown in Equation (5).

$$Y = \mathrm{Conv}_{1\times1}(M) + X \tag{5}$$

Herein, $Y \in \mathrm{R}^{B\times C\times H\times W}$ is the output feature map of the module, whose dimensions and number of channels are exactly the same as those of the input.

3.2. Inception-V3 of the Proposed ResiDS-Net Based Power Outage Risk Perception Method for Medium- and Low-Voltage Distribution Networks

Inception-V3 is a high-performance convolutional neural network proposed by the Google Brain team. It can significantly enhance multi-scale feature extraction capability while maintaining high computational efficiency, and has become one of the most widely used backbone networks in the field of computer vision. Inception-V3 consists of a Stem layer, 11 cascaded Inception modules, and a global average pooling classification head. Its core design concept is to realize the simultaneous extraction and fusion of features at different scales through a parallel multi-branch architecture. Each Inception module contains four parallel branches: 1×1 pointwise convolution, 3×3 convolution, 5×5 convolution, and average pooling. These can simultaneously capture image features with different receptive fields and enable the accurate perception of multi-scale targets [20].

To further reduce computational complexity and improve feature representation capability, Inception-V3 adopts the convolution factorization technique. It decomposes a 5×5 convolution into two consecutive 3×3 convolutions, and further decomposes a 3×3 convolution into a combination of 1×3 and 3×1 asymmetric convolutions. This significantly reduces computational cost while maintaining the same receptive field, and simultaneously increases the nonlinear representation capability of the network [21]. In addition, the model introduces auxiliary classifiers in the intermediate layers to provide additional gradient supervision signals during training, which effectively alleviates the vanishing gradient problem in deep networks. Through the label smoothing regularization technique, the generalization capability of the model is significantly improved [22]. The Inception module is shown in Figure 3, and the structure of Inception-V3 is shown in Figure 4.

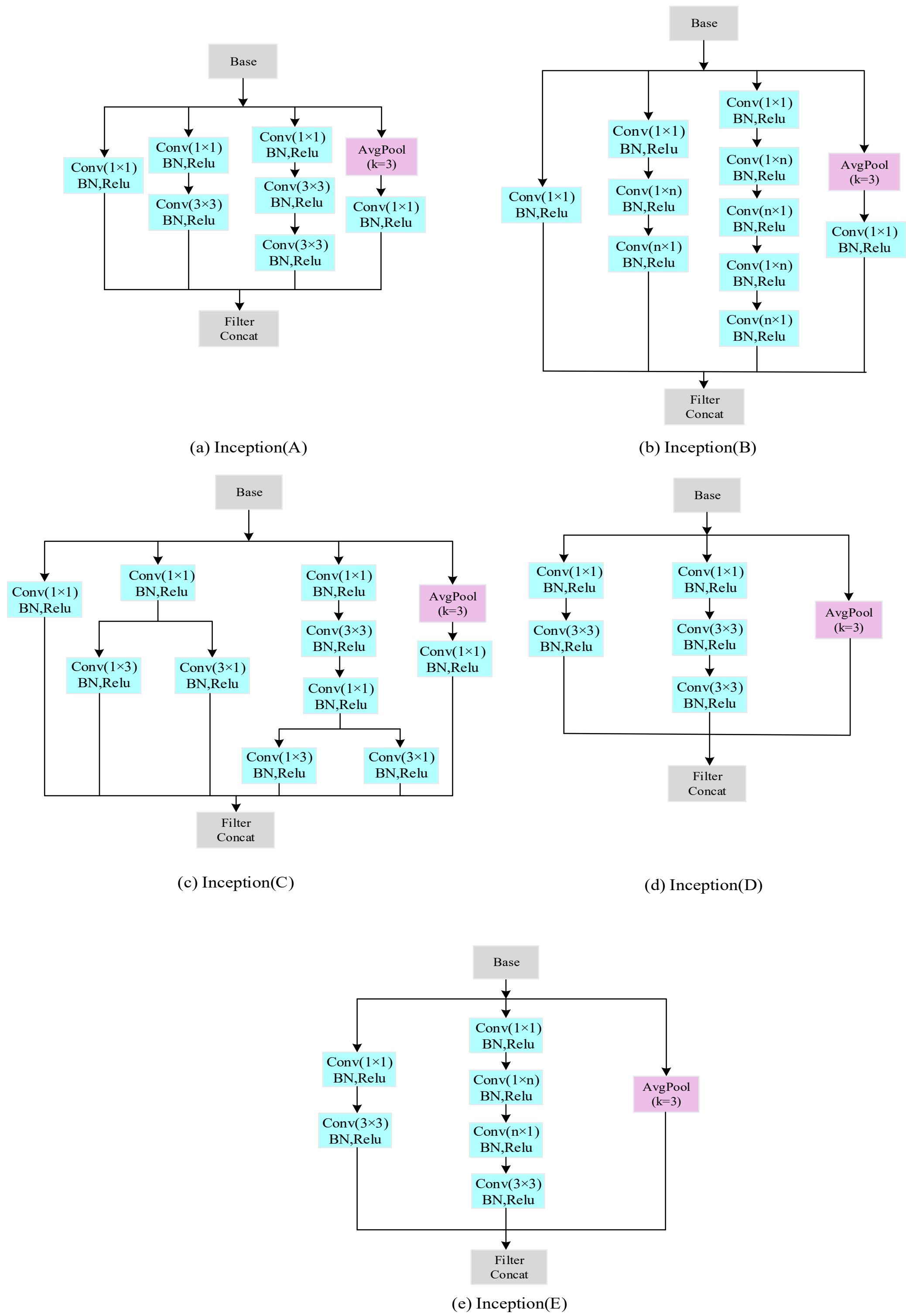

Figure 3. Structure of the Inception module.

3.3. DenseNet121 of the Proposed ResiDS-Net Based Power Outage Risk Perception Method for Medium- and Low-Voltage Distribution Networks

DenseNet121 is a high-performance convolutional neural network. With its innovative dense connection mechanism, it has become one of the classic backbone networks in the field of computer vision. The core design concept of this network is to achieve deep feature reuse by establishing dense connections between layers. This effectively addresses the vanishing gradient problem and feature information waste inherent in traditional deep convolutional neural networks, and reduces the number of parameters and computational complexity of the model while maintaining high detection accuracy [23].

DenseNet121 consists of a 7 × 7 convolutional layer, four cascaded Dense Blocks, and three alternating Transition Layers. Each Dense Block contains multiple convolutional units, with direct connection paths between any two units. The input of each layer is the concatenation of feature outputs from all preceding layers [24]. Such dense connections enable the network to fully exploit hierarchical feature information and allow gradients to flow directly from the output layer to any earlier layer, greatly improving the training stability of deep networks. The Transition Layers between Dense Blocks compress the number of channels and spatial size of feature maps through 1 × 1 convolution and average pooling, further reducing computational cost [25]. In addition, DenseNet121 adopts a pre-activation structure composed of batch normalization, ReLU activation, and convolutional layers, which further optimizes feature propagation and accelerates model convergence [26]. The structure of DenseNet121 is shown in Figure 5, and the structure of the Dense Block in DenseNet121 is shown in Figure 6. Figure 6. Dense block structural diagram, where different colored lines denote skip connections from different preceding bottleneck layers.

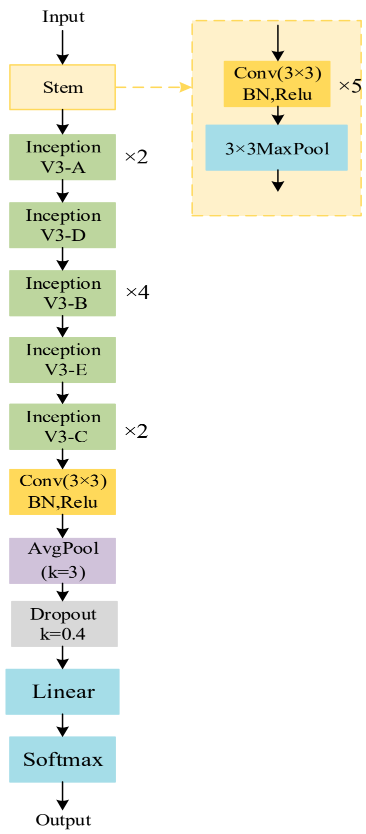

Figure 4. Structure of the Inception-V3.

3.4. Improved Dempster–Shafer Evidence Theory of the Proposed ResiDS-Net Based Power Outage Risk Perception Method for Medium- and Low-Voltage Distribution Networks

The traditional DS evidence theory has three inherent defects in multi-source heterogeneous data fusion scenarios, namely, the Basic Probability Assignment (BPA) is prone to distortion due to noise interference, it defaults to equal weights for all evidence sources, and high-conflict evidence fusion easily produces counterintuitive decision paradoxes. These defects make it difficult to adapt to the complex environment of distribution network power outage risk perception after typhoon disasters [27]. To address this issue, this study proposes an improved DS evidence theory fusion method for multi-source deep learning features [28]. It systematically solves the above defects through a four-stage process consisting of error-corrected BPA normalization, the adaptive weighting of evidence credibility, conflict-optimized fusion rule, and decision probability conversion, achieving the robust fusion of multi-model decision results.

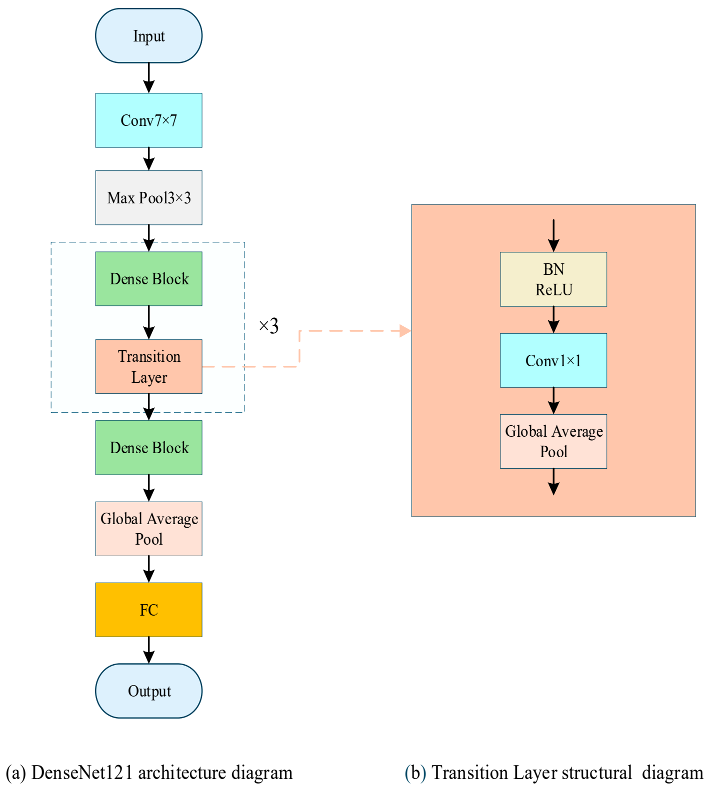

Figure 5. Structure of the DenseNet121.

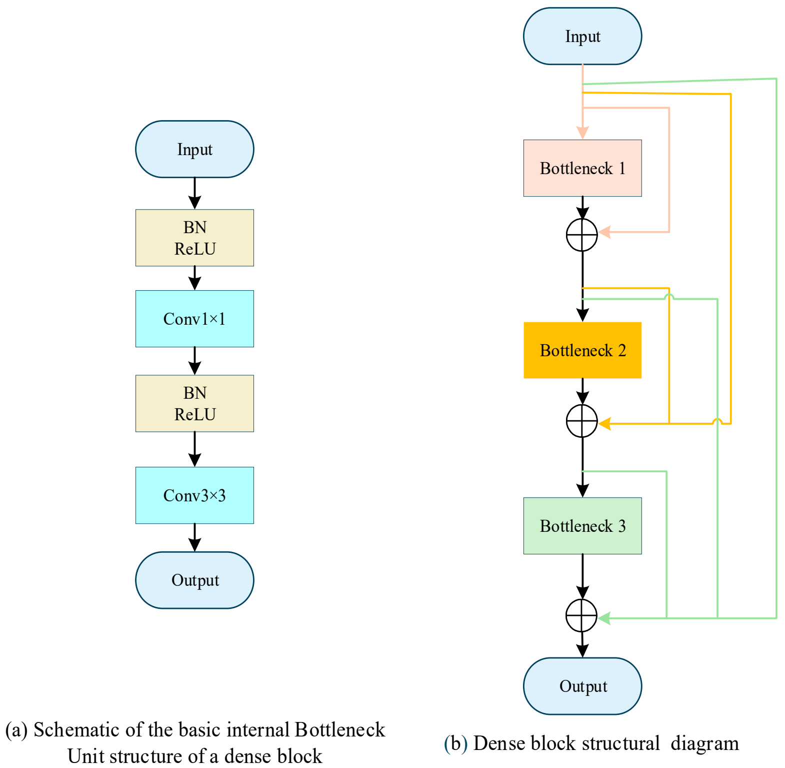

Figure 6. Schematic diagram of the Dense block in DenseNet121.

Let the frame of discernment be denoted as $\Theta = \{\theta_1, \theta_2, \ldots, \theta_c\}$, where C is the total number of distribution network operational state categories, and θ_c represents the c-th operational state. In this study, a total of $S = 3$ independent evidence sources are established, corresponding to the Softmax output results from the three parallel branches, namely, CM-ResNet50, Inception-V3, and DenseNet121.

To overcome the limitation of traditional DS theory, which directly adopts Softmax probabilities as BPA while ignoring the inherent prediction noise of each model, this study introduces a class-specific model output error e_i^j as a correction term. This error is computed as the mean absolute error of the model on the validation set, as formulated in Equation (6).

$$e_i^j = \frac{1}{N}\sum_{k=1}^{N}\left|y_{true,k}^j - y_{pred,i,k}^j\right|, i = 1,2,\ldots,S; j = 1,2,\ldots,C \tag{6}$$

where N is the total number of validation samples, $y_{true,k}^j$ is the ground-truth label of the k-th validation sample for class j, and $y_{pred,k}^j$ is the Softmax probability assigned by the i-th model to the k-th validation sample for class j. This error term is class-specific, reflecting the model's varying discriminative ability across different categories rather than applying a uniform correction to all classes.

Based on the above class-specific errors, the basic belief assignment $m_i(\{\theta_j\})$ of the i-th evidence source for the singleton state set $\{\theta_j\}$ is computed as shown in Equation (7).

$$m_i(\{\theta_j\}) = \frac{p_i^j}{1 + e_i^j}, i = 1,2,\ldots,3; j = 1,2,\ldots,C \tag{7}$$

where p_i^j is the Softmax output probability of the i-th evidence source for predicting the input sample as class j.

Meanwhile, to explicitly model the prediction uncertainty, the remaining belief mass is assigned to the full set Θ, representing the overall uncertainty when the model cannot determine a specific category, as computed in Equation (8).

$$m_i(\{\Theta\}) = 1 - \sum_{j=1}^{C} m_i(\{\theta_j\}) = 1 - \sum_{j=1}^{C}\frac{p_i^j}{1 + e_i^j}, i = 1,2,\ldots,S \tag{8}$$

Clearly, for any evidence source i, $m_i(\{\Theta\}) + \sum\limits_{j=1}^{C} m_i(\{\theta_j\}) = 1$ holds, satisfying the fundamental normalization requirement of DS evidence theory. The physical interpretation of this generation strategy is clear: when the prediction error e_i^j of a model for a particular class is small, $m_i(\{\theta_j\})$ becomes larger, indicating that the model's judgment for that class is reliable; conversely, when the error is large, the belief assignment is automatically suppressed. Meanwhile, all belief mass reduced due to errors is uniformly allocated to the full set Θ as the model's cognitive uncertainty for that sample, effectively preventing noise from interfering with the subsequent fusion process.

Traditional DS theory defaults to equal weights for all evidence sources, failing to accommodate the varying quality of different data sources in practical scenarios. This study quantifies the consistency among different model outputs by calculating the cosine similarity between evidence vectors.

For the p-th and q-th evidence sources $(p, q \in \{1, 2, \ldots, S\}, p \neq q)$, their BPA vectors are $m_p = \left[m_p(\{\theta_1\}), \ldots, m_p(\{\theta_C\}), m_p(\Theta)\right]$ and $m_q = \left[m_q(\{\theta_1\}), \ldots, m_q(\{\theta_C\}), m_q(\Theta)\right]$, respectively. The similarity coefficient S_{pq} between them is defined in Equation (9), as follows:

$$S_{pq} = \frac{m_p \cdot m_q}{\|m_p\| \cdot \|m_q\|}, p, q \in \{1, 2, \ldots, S\}, p \neq q \tag{9}$$

where $S_{pq} \in [0, 1]$. A coefficient closer to 1 indicates greater consistency between the two evidence sources in judging the distribution network state, implying higher credibility. Based on the similarity coefficients, the global support degree S_{up_p} received by the p-th evidence source from all other evidence sources is calculated as shown in Equation (10).

$$S_{up_p} = \sum_{q=1, q \neq p}^{S} S_{pq}, p = 1, 2, \ldots, S \tag{10}$$

Subsequently, the global support degree is normalized to obtain the adaptive credibility weight w_p for each evidence source, as shown in Equation (11).

$$w_p = \frac{S_{up_p}}{\sum_{\tau}^{S} S_{up_r}}, p = 1, 2, \ldots, S \tag{11}$$

Clearly, $\sum_{p=1}^{S} w_p = 1$ and $w_p \in [0, 1]$. This adaptive weighting mechanism dynamically responds to quality variations among data sources. When a model produces biased predictions due to cloud occlusion or noise interference, its consistency with other models decreases, the global support degree automatically diminishes, and the credibility weight is correspondingly reduced, enabling dynamic evidence source selection without manual intervention.

To address the decision paradox problem that arises when traditional DS combination rules process highly conflicting evidence, this study proposes an improved weighted conflict fusion rule that jointly optimizes the adaptive credibility weights and the evidence conflict coefficient [29]. First, the global conflict coefficient K among all evidence sources is computed to quantify the overall degree of conflict among multi-source evidence, as formulated in Equation (12), as follows:

$$K = \sum_{\cap_{I=1}^{S} Ai = \varnothing} \prod_{i=1}^{S} m_i(A_i) \tag{12}$$

where A_i denotes the state subset claimed by the i-th evidence source, which can be a singleton set θ_j or the full set Θ. $K \in [0, 1]$. A larger value of K indicates stronger conflict among the evidence sources. Subsequently, the conflict coefficient K and the credibility weights w_i are used to revise the fusion rule. For any state subset $A \subseteq \Theta$, the fused belief assignment $m_{fused}(A)$ is computed as shown in Equation (13).

$$m_{fused}(A) = \frac{\sum_{\cap_{i=1}^{S}} [w_i \cdot m_i(A_i)]}{1 - K \cdot \sum\limits_{i=1}^{S} (1 - w_i)} \tag{13}$$

The key advantages of this improved rule are twofold. On the one hand, w_i adaptively reduces the contribution of unreliable evidence, mitigating its negative impact on the fusion outcome. On the other hand, the term $1 - K \cdot \sum\limits_{i=1}^{S} (1 - w_i)$ in the denominator makes the penalty degree of the conflict coefficient K depend on the fusion result coupled with the overall credibility of the evidence. When the overall evidence credibility is high $\sum w_i \approx S$, even if some conflict exists $K > 0$, the fusion result can still effectively preserve the consensus information among all evidence sources. When the overall evidence credibility is low, the penalty effect of conflict is enhanced, thereby avoiding the shortcomings of traditional methods that either simply discard conflicting evidence or produce counterintuitive conclusions.

Traditional DS theory outputs belief assignments at the set level, which cannot be directly used for final class-level decision-making. This study converts the fused BPA into single-class decision probabilities. For the j-th class state θ_j, the decision probability $P(\theta_j)$ is defined as in Equation (14).

$$P(\theta_j) = m_{fused}(\{\theta_j\}) + \frac{1}{C} \cdot m_{fused}(\Theta), j = 1, 2, \ldots, C \tag{14}$$

This conversion evenly distributes the uncertain mass of the full set Θ among all categories, ensuring the normalization of decision probabilities $\sum_{j=1}^{C} P(\theta_j) = 1$. Finally, the state category with the maximum decision probability is selected as the power outage risk perception result for the input image, as expressed in Equation (15).

$$\theta_{final} = arg \max_{1 \leq j \leq C} P(\theta_j) \tag{15}$$

The proposed multi-model fusion method based on improved DS evidence theory is fundamentally different from traditional ensemble learning methods such as weighted averaging, majority voting, or Stacking. Weighted averaging and majority voting only utilize the final hard decisions or raw probabilities of models for linear combination, failing to leverage the uncertainty information in model outputs and exhibiting limited capability in handling conflicting evidence. Stacking, as a meta-ensemble method, relies on an additional learner to learn the combination strategy, and its performance is highly dependent on the design and training data of the meta-learner, with relatively poor interpretability.

3.5. ResiDS-Net for Power Outage Risk Perception in Medium- and Low-Voltage Distribution Networks

The principle of the ResiDS-Net model is shown in Figure 7. ResiDS-Net combines the classification score matrices of CM-ResNet50, Inception-V3, and DenseNet121, and improves the prediction accuracy for medium- and low-voltage distribution networks using the improved DS evidence theory. The flow chart of power outage risk perception for medium- and low-voltage distribution networks based on the proposed ResiDS-Net is shown in Figure 8.

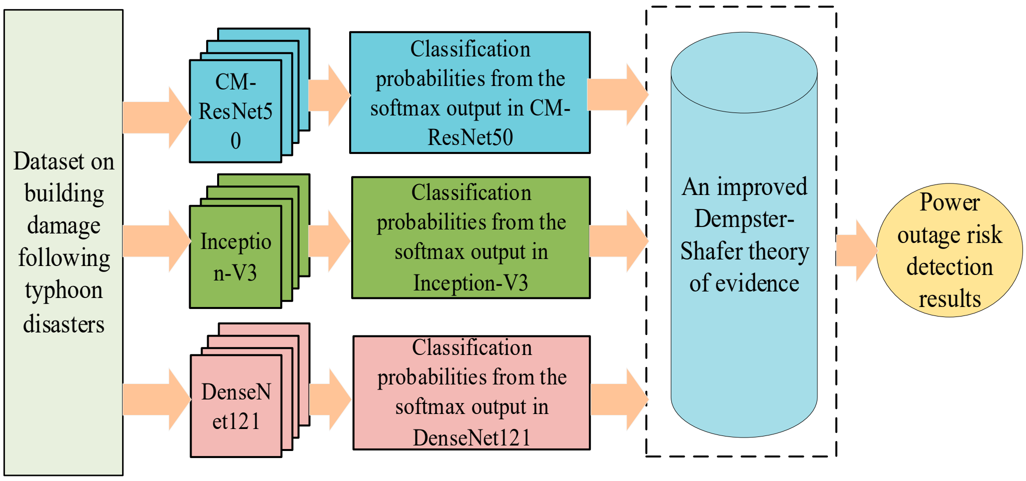

Figure 7. Schematic diagram of the proposed ResiDS-Net.

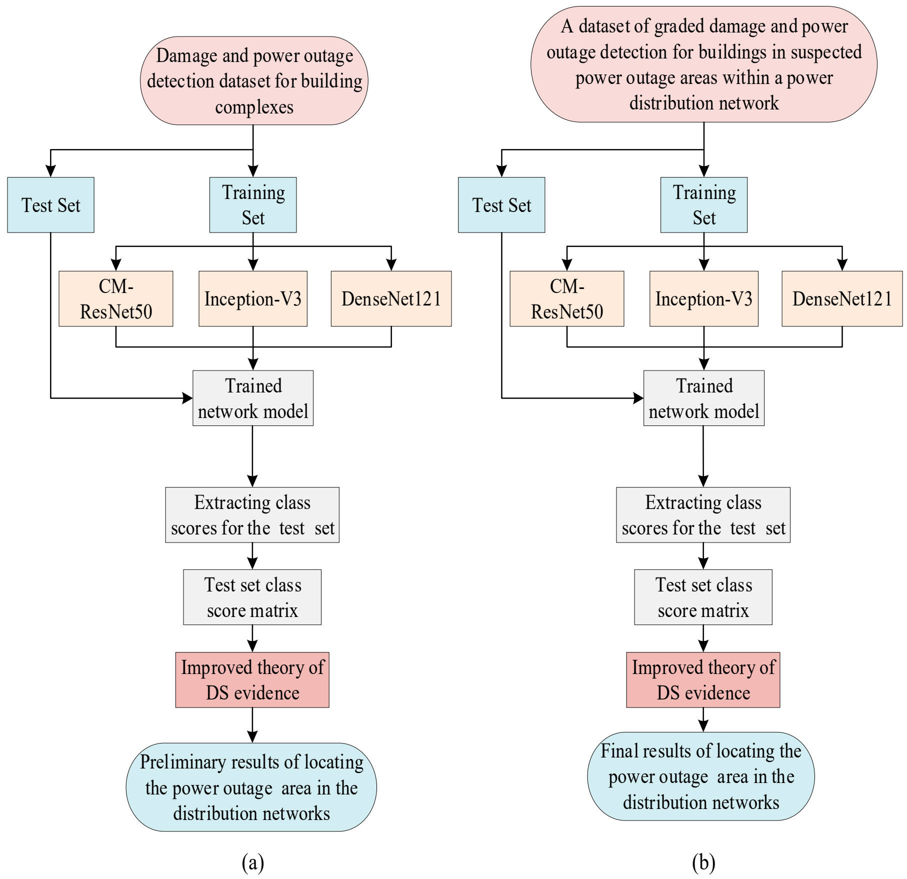

Figure 8. Flowchart of distribution network outage risk perception based on ResiDS-Net. (**a**) Initial outage risk perception process; (**b**) Final outage risk perception process.

The flow of power outage risk perception for medium- and low-voltage distribution networks using the proposed ResiDS-Net is as follows:

1. Convert the building damage and power outage risk perception dataset after typhoon disasters from TIFF format to PNG format, and classify the data into two categories, damaged and undamaged, according to whether damaged buildings exist in the images;
2. Resize the converted satellite image dataset from 1024 × 1024 to 224 × 224;
3. Feed the training set into the CM-ResNet50, Inception-V3 and DenseNet121 network models for training. The Adam optimizer is adopted as the training optimizer. The three networks are trained in parallel to improve training efficiency;
4. Input the test set into the well-trained CM-ResNet50, Inception-V3 and DenseNet121 networks to obtain the category score matrices of the test set for the three networks. The category score matrices are fused via the improved DS evidence theory to obtain the preliminary perception result of post-typhoon building damage and power outage risk areas;
5. Input the training set of the building graded damage and power outage risk perception dataset for post-typhoon buildings, which contains preliminarily identified power outage areas, into the CM-ResNet50, Inception-V3 and DenseNet121 network models for training. The Adam optimizer is adopted as the training optimizer;
6. Feed the test set into the well-trained CM-ResNet50, Inception-V3 and DenseNet121 networks to acquire the category score matrices of the test set for the three networks. The category score matrices are fused through the improved DS evidence theory, and

the final perception result of post-typhoon building damage and power outage risk areas is obtained according to building damage levels.

The major features of the proposed method can be summarized as follows:

1. Aiming at the problems of performance degradation, feature loss and time-consuming training caused by excessive depth in traditional serial deep learning networks, the proposed ResiDS-Net adopts a parallel architecture, which synchronously extracts multi-scale features through three sub-networks and effectively reduces the loss of critical information;
2. The proposed ResiDS-Net fuses the noise-robust deep feature extraction of CM-ResNet50, the multi-scale feature capture capability of Inception-V3, and the fine-grained feature reuse capability of DenseNet121 via the improved DS evidence theory, which can improve the localization accuracy of power outage risk areas;
3. To address the issues of traditional DS evidence theory in multi-source fusion, including vulnerable belief assignment disturbed by noise, equal weight setting, and decision paradoxes easily caused by conflicting evidence, this study proposes an improved DS evidence method [30]. It standardizes belief assignment through error correction, adaptively assigns weights based on similarity and support degree, optimizes the conflict fusion rule, and adds decision probability conversion, which allows it to better adapt to the characteristics of multi-source heterogeneous data in distribution networks;
4. On the basis of ResNet50, this study proposes a Conv Modulation module and constructs CM-ResNet50. This module stabilizes feature distribution through layer normalization, captures global context via large-kernel depthwise convolution, and adopts GELU activation and dual-branch element-wise self-modulation. It enhances the network's ability to focus on deep damage features and the noise robustness for remote sensing images, making up for the shortcomings of ResNet50 such as sensitivity to cloud and fog interference and the insufficient expression of fine-grained damage features.

4. Case Studies

In this experiment, the hardware configuration includes an AMD Ryzen 7 7735H processor, 16 GB of RAM, and an NVIDIA RTX 4060 graphics card, running on a 64-bit Windows 11 operating system. All network models used in this section are implemented using Python 3.13 combined with the PyTorch 1.12 framework. Verification is conducted on the post-typhoon building damage and power outage risk perception dataset and the post-typhoon building graded damage and power outage risk perception dataset. ResiDS-Net is compared with nine classic models including ResNet50, as shown in Table 6. During the experiments, all networks are trained with GPU acceleration, the Adam optimizer is adopted, the learning rate is set to 0.0001, and the batch size is set to 32. For the post-typhoon building damage and power outage risk perception dataset, the training set contains 2382 images, the validation set contains 817 images, and the test set contains 749 images. For the post-typhoon building graded damage and power outage risk perception dataset, the training set contains 2790 images, the validation set contains 400 images, and the test set contains 800 images.

4.1. Preliminary Power Outage Risk Perception of Building Damage After Typhoon Disasters

In the post-typhoon building damage and power outage risk perception dataset, the training set contains 2382 images, the validation set contains 817 images, and the test set contains 749 images. The accuracy curves and loss function curves generated from the training of all comparison algorithms are plotted below, as shown in Figure 9.

Table 6. Comparison of network models.

Name	Input	Parameters (M)	Layers
ResiDS-Net	224 × 224 × 3	68.14	624
CM-ResNet50	224 × 224 × 3	36.36	188
ResNet50 [31]	224 × 224 × 3	25.40	176
DenseNet121 [32]	224 × 224 × 3	7.98	121
Inception-V3 [33]	224 × 224 × 3	23.80	315
VGG16 [34]	224 × 224 × 3	138.30	41
VGG19 [35]	224 × 224 × 3	143.60	47
ConvNeXt [36]	224 × 224 × 3	188.66	136
ResNet101 [37]	224 × 224 × 3	44.70	347
GhostNet-V2 [38]	224 × 224 × 3	5.30	257

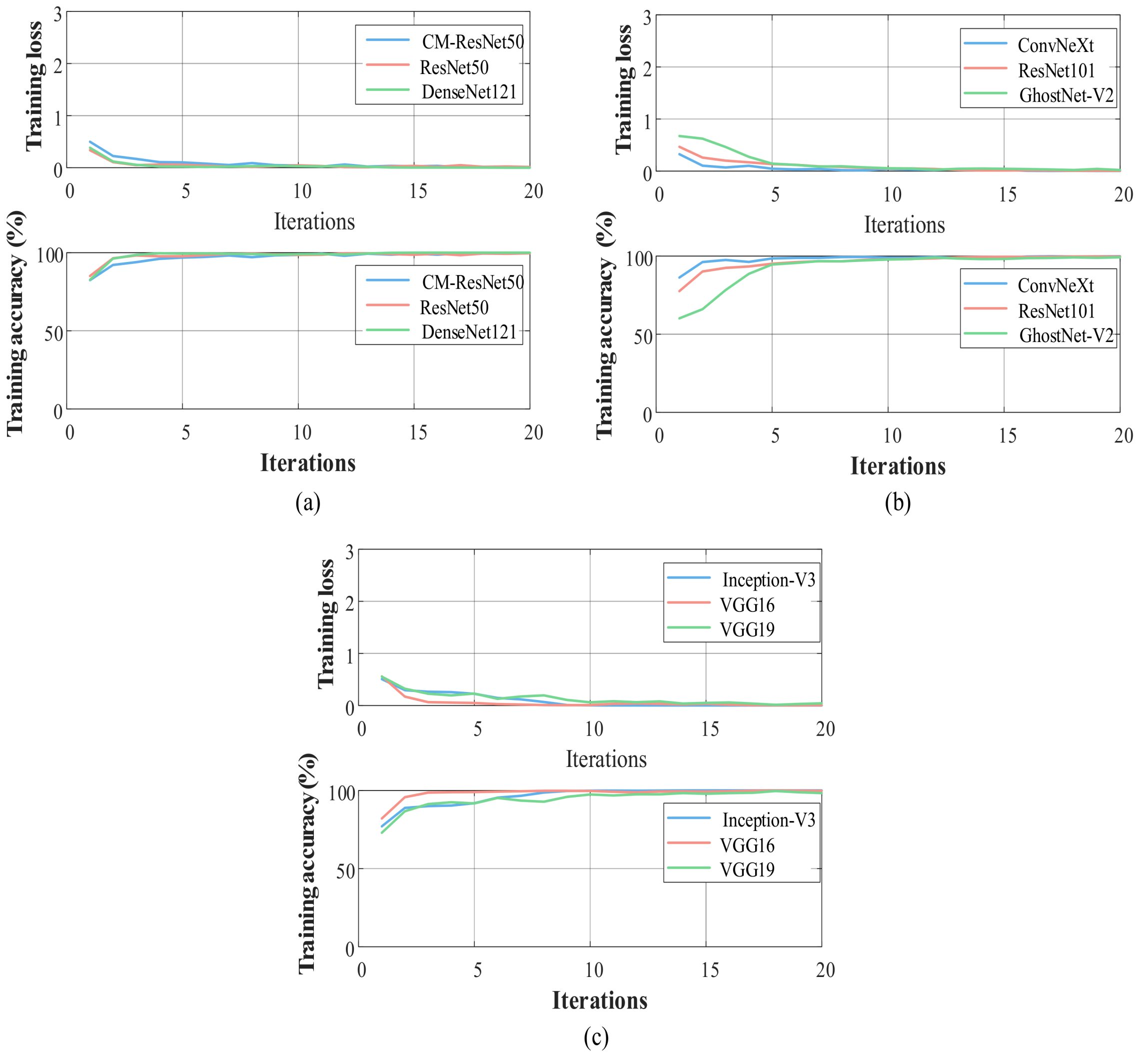

Figure 9. Training loss and training accuracy curves of 9 algorithms: (**a**) CM-ResNet50, ResNet50, DenseNet121; (**b**) ConvNeXt, ResNet101, GhostNet-V2; (**c**) Inception-V3, VGG16, VGG19.

The training time and test results of each network are shown in Table 7.

ResiDS-Net achieves the best performance on all evaluation metrics in the post-typhoon building damage and power outage risk perception task, while DenseNet121 achieves the second-best results. ResiDS-Net achieves an accuracy of 96.66%, an F1 score of 95.57%, and a precision of 96.43%, which are 2.13%, 2.83%, and 2.86% higher than those of DenseNet121, respectively. The training time of ResiDS-Net is 2963.70 s, with a moderate training duration. It is only 0.11 s longer than the Inception-V3 branch, which takes the longest training time among the sub-networks in ResiDS-Net. CM-ResNet50 with the introduced Conv Modulation module achieves an accuracy of 93.99%, an F1 score of 92.17%, and a precision of 91.38%, which are 1.33%, 1.60%, and 2.79% higher than those of ResNet50, respectively. This demonstrates that the introduction of the Conv Modulation module enhances the ability of the ResNet50 network to focus on deep damage features.

Table 7. Training and test results with the Adam optimizer.

Name	F1 Score (%)	Precision (%)	Test Accuracy (%)	Train Time (s)	Inference Time (ms)
ResiDS-Net	**95.57**	**96.43**	**96.66**	**2963.79**	**2.02**
CM-ResNet50	92.17	91.38	93.99	2390.50	0.67
ResNet50	90.57	88.59	92.66	2341.55	0.56
DenseNet121	92.74	93.57	94.53	2378.08	1.86
Inception-V3	91.44	89.30	93.32	2963.68	1.99
VGG16	90.12	89.04	92.39	3628.40	1.62
VGG19	89.62	93.18	92.39	3825.60	2.05
ConvNeXt	93.12	92.15	93.46	3440.98	2.85
ResNet101	92.20	93.19	94.13	4995.04	1.01
GhostNet-V2	50.32	65.00	69.16	2325.8	0.44

In this study, inference time is a metric that measures the time taken for a single 224×224-pixel satellite image to be processed from model input to the power outage risk assessment result, expressed in milliseconds. It provides an intuitive reflection of the model's actual response speed at an emergency scene. As shown in Table 7, the single-image inference times for all comparison networks are in the millisecond range, demonstrating rapid output capabilities. Among them, ResiDS-Net—which integrates three parallel feature extraction branches and an improved DS evidence theory fusion module—takes 2.02 ms for single-image inference. While this is slightly higher than most single-backbone networks, it still remains at an extremely low millisecond level overall. Although there is a slight increase in inference time, the accuracy improvement achieved by ResiDS-Net is significant, with an accuracy rate 2.13% higher than that of the best single model, effectively reducing the risk of misclassifications and missed detections after a disaster. From the perspective of actual emergency response needs, a single-image inference speed in the two-millisecond range fully meets the requirements for near-real-time detection. Even with batch-processing remote sensing image tiles covering large areas, it can quickly perform a preliminary assessment of power outage areas following a typhoon, striking a balance between accuracy and efficiency.

To more intuitively demonstrate the superior performance of ResiDS-Net in the post-typhoon building damage and power outage risk perception task, this study adopts confusion matrices and Receiver Operating Characteristic (ROC) curves to visualize the classification results, as shown in Figures 10 and 11, respectively.

Figure 10 shows the binary classification confusion matrix, which intuitively presents the distribution of classification results of the model for samples in two types of regions, namely, no building damage and building damage, where no building damage corresponds to normal power supply areas and building damage corresponds to suspected outage-risk areas. Among them, true negatives (TNs) represent the number of region samples that are actually free of building damage and predicted as undamaged by the model, that is, the number of correctly identified building regions with normal power supply; false positives (FPs) represent the number of region samples that are actually free of building damage but misclassified as damaged, corresponding to the misjudgment of normal power supply areas as power outage areas; true positives (TPs) represent the number of region samples that actually have building damage and are predicted as damaged by the model, that is, the number of accurately detected high outage risk areas with building damage, and false negatives (FNs) represent the number of region samples that actually have building damage but misclassified as undamaged, corresponding to the missed judgment of damaged power outage risk areas as normal power supply areas.

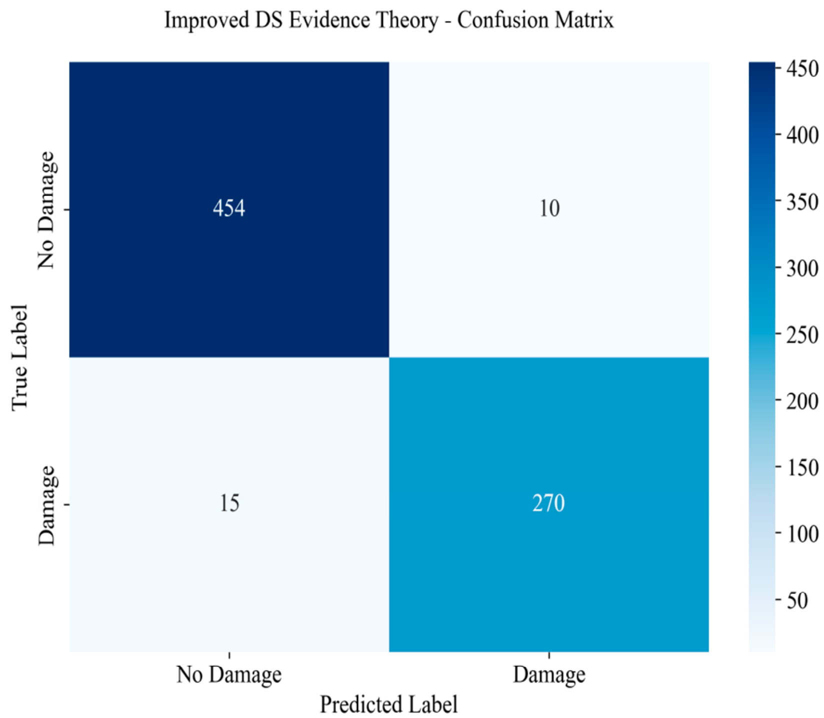

Figure 10. Confusion matrix of ResiDS-Net.

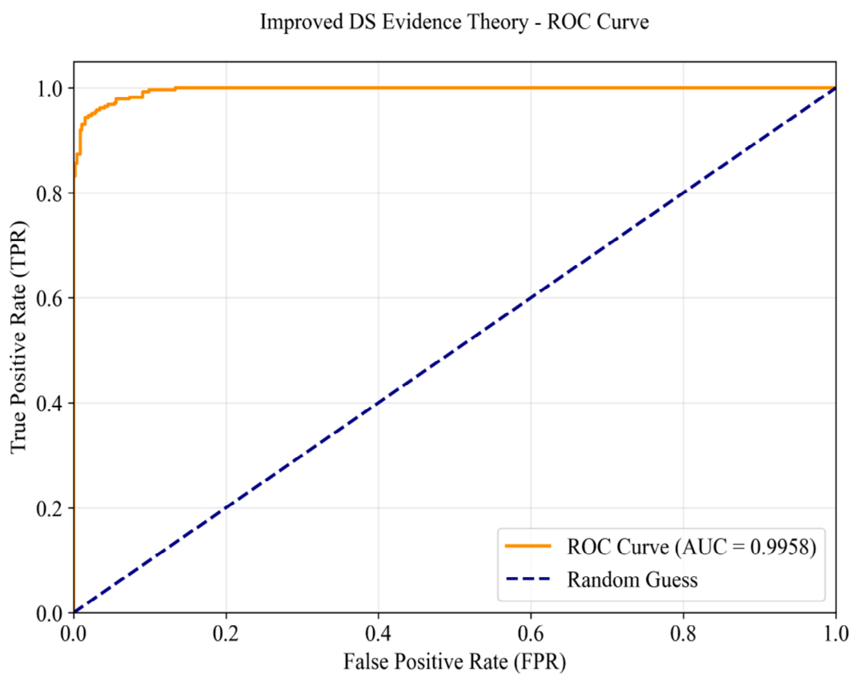

Figure 11. ROC curve of ResiDS-Net.

It can be seen from Figure 10 that the number of true negatives (TNs) is 454, that of false positives (FP) is 10, that of true positives (TP) is 270, and that of false negatives (FN) is 15. The ROC curve in Figure 11 takes the false positive rate (FPR) as the horizontal axis and the true positive rate (TPR) as the vertical axis, and the blue dashed line passing through the origin represents the random guess curve; the larger the area under the curve (AUC) and the farther the curve is above the random guess line, the better the classification performance of the model, where the AUC value of ResiDS-Net can reach 0.9958.

4.2. Graded Damage and Power Outage Risk Perception of Buildings After Typhoon Disasters

In the post-typhoon building graded damage and power outage risk perception dataset, the training set contains 2790 images, the validation set contains 400 images, and the test set contains 800 images. The accuracy curves and loss function curves generated from the training of all comparison algorithms are plotted below, as shown in Figure 12.

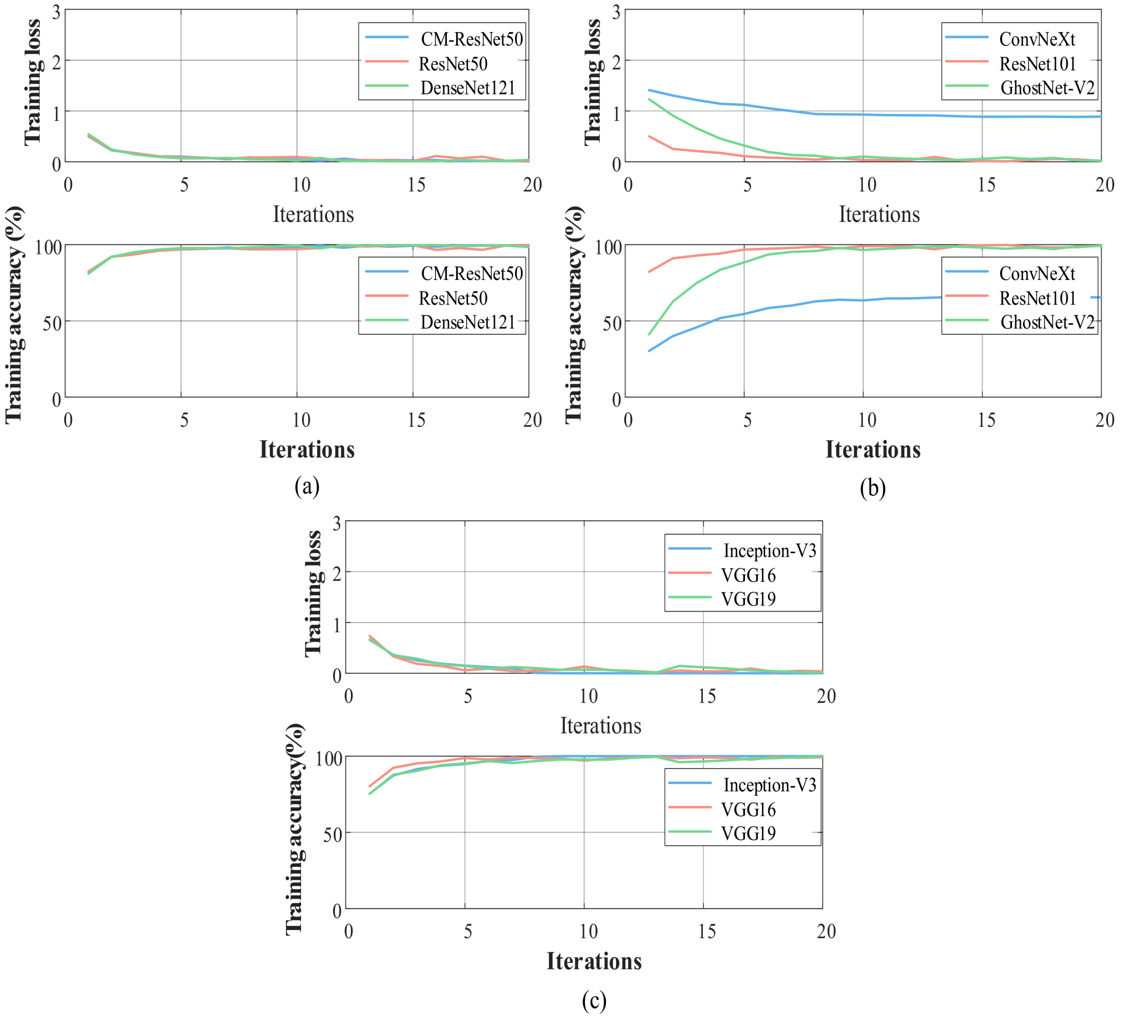

Figure 12. Training loss and training accuracy curves of 9 algorithms: (**a**) CM-ResNet50, ResNet50, DenseNet121; (**b**) ConvNeXt, ResNet101, GhostNet-V2; (**c**) Inception-V3, VGG16, VGG19.

The training time and test results of each network are shown in Table 8. The bolded sections in Table 8 are intended to better illustrate the performance of the proposed ResiDS-Net method.

ResiDS-Net achieves the best performance on all evaluation metrics in the post-typhoon building graded damage and power outage risk perception task, while CM-ResNet50 achieves the second-best results. ResiDS-Net achieves an accuracy of 93.00%, an F1 score of 92.89% and a precision of 93.07%, which are 2.50%, 2.55% and 2.64% higher than those of CM-ResNet50, respectively. The training time of ResiDS-Net is 679.03 s with a moderate training duration, which is only 0.22 s longer than that of the Inception-V3 branch, the sub-network with the longest training time in ResiDS-Net. CM-ResNet50 integrated with the Conv Modulation module obtains an accuracy of 90.50%, an F1 score of 90.34% and a precision of 90.43%, which are 2.12%, 1.96% and 2.64% higher than those of ResNet50, respectively, demonstrating that the introduction of the Conv Modulation module enhances the ability of the ResNet50 network to focus on deep damage features.

Table 8. Training and test results with the Adam optimizer.

Name	F1 Score (%)	Precision (%)	Test Accuracy (%)	Train Time (s)	Inference Time (ms)
ResiDS-Net	**92.89**	**93.07**	**93.00**	**679.03**	**1.52**
CM-ResNet50	90.34	90.43	90.50	470.44	0.62
ResNet50	88.38	89.23	88.38	449.53	0.57
DenseNet121	88.93	89.29	89.12	450.95	1.33
Inception-V3	88.33	88.50	88.50	678.81	0.89
VGG16	87.05	87.81	87.25	825.45	0.26
VGG19	87.48	88.12	87.62	1014.14	0.28
ConvNeXt	57.10	57.54	58.25	1038.82	1.89
ResNet101	89.06	89.52	89.25	2387.18	0.75
GhostNet-V2	58.06	61.86	58.00	242.51	0.422

CM-ResNet50 requires a training time of 470.44 s, which is only 20.91 s longer than ResNet50 and far less than the 2387.18 s required for ResNet101 training, while its accuracy is 1.25% higher than that of ResNet101.

In the fine-grained building damage grading and power outage risk perception task, inference time refers to the end-to-end latency of a single 224 × 224-pixel building slice, from model input to the output of a four-level damage grade prediction. Measured in milliseconds, it directly reflects the actual response efficiency of the second-stage fine review process. The results show that single-image inference for all comparison networks remains at the millisecond level, demonstrating competent rapid grading capabilities. Benefiting from the integration of three-branch parallel feature extraction and improved DS evidence theory fusion, ResiDS-Net achieves a single-image inference latency of 1.52 ms. Although this value is slightly higher than that of most single-backbone networks, it still falls within an extremely low latency range overall. Notably, its inference speed outperforms the ConvNeXt model, which has a larger parameter scale, namely, the inference latency is reduced by 0.37 ms (a 19.6% decrease) compared to ConvNeXt. This fully validates the effectiveness of the parallel fusion architecture in efficiency management, indicating that the multi-branch parallel design does not result in excessive efficiency loss. Despite the minor increase in inference latency relative to lightweight single models, ResiDS-Net improves accuracy by 2.50% over the optimal single model in the more challenging fine-grained damage grading task, effectively reducing misjudgments of power outage risk caused by incorrect damage grade classification. Combined with the logic of the two-stage perception framework—where this stage performs only secondary assessment on suspected outage areas screened in the first stage—the scale of samples to be processed is significantly reduced. The millisecond-level inference speed fully supports near-real-time and accurate post-disaster power outage risk assessment, which aligns well with the practical decision-making requirements of emergency repairs.

To more intuitively demonstrate the superior performance of ResiDS-Net in the post-typhoon building graded damage and power outage risk perception task, this study uses confusion matrices and Receiver Operating Characteristic (ROC) curves to visualize the classification results, as shown in Figures 13 and 14, respectively.

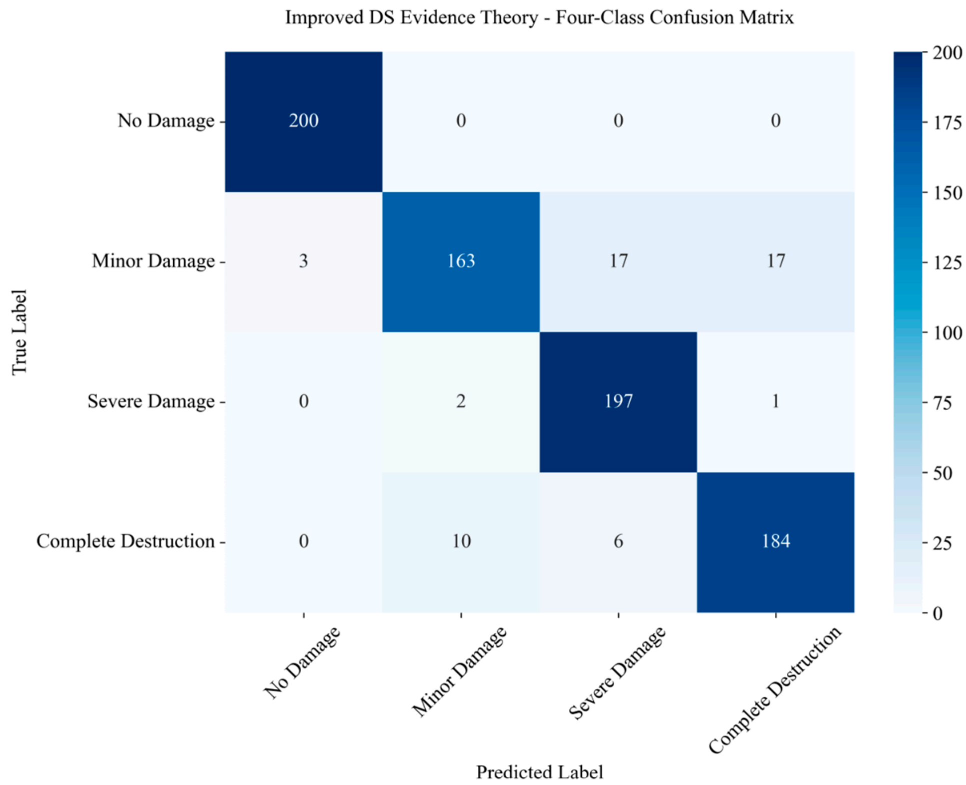

Figure 13. Confusion matrix of ResiDS-Net.

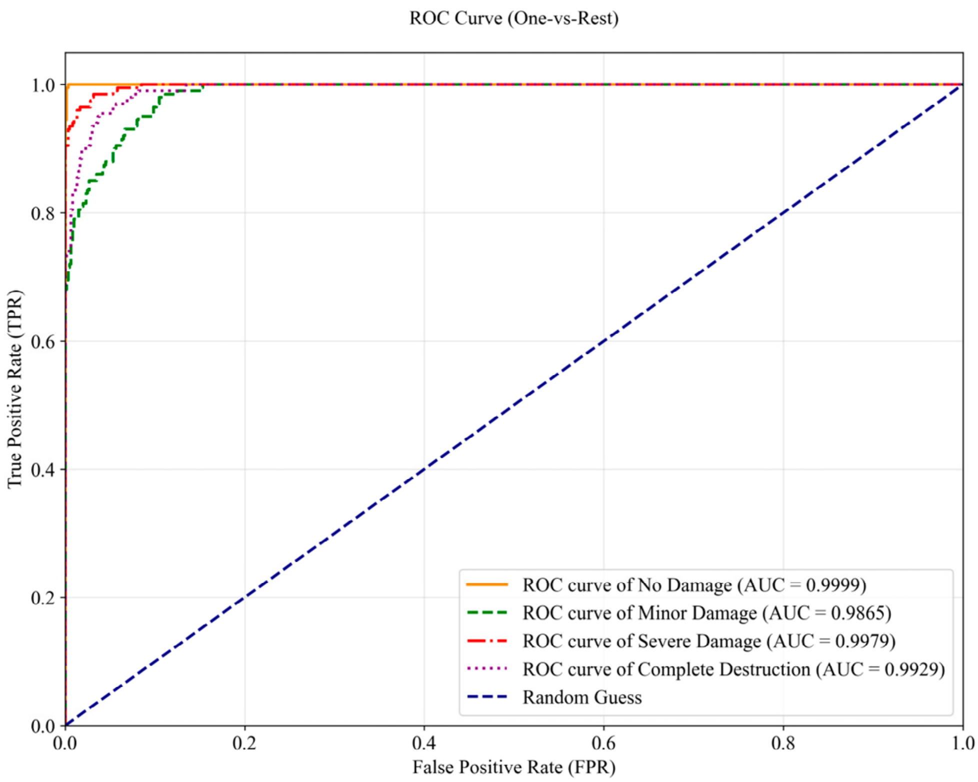

Figure 14. ROC curve of ResiDS-Net.

Figure 13 shows the four-class confusion matrix, which intuitively presents the distribution of grading results of the model for four types of building damage samples, as follows: no damage, minor damage, severe damage and complete destruction. In this task, the building damage degree is divided into four mutually exclusive and progressive levels, corresponding to different power outage risk probabilities respectively. No damage corresponds to a power outage risk probability of 0, minor damage refers to non-structural building damage with negligible outage risk, major damage corresponds to a high outage risk probability, and destruction corresponds to an outage risk probability of 1. The diagonal elements of the matrix correspond to the true positives of each category, namely, the number of region samples where the true labels are completely consistent with the model prediction results. The off-diagonal elements correspond to various misclassified samples. The off-diagonal elements in the row direction are the false negatives of the category, representing the number of building samples that actually belong to a certain damage level but are incorrectly judged as other levels by the model, and the off-diagonal elements in the column direction are the false positives of the category, representing the number of building samples that do not actually belong to the damage level but are misclassified into this category. Taking the no building damage category as an example, its true positives correspond to the number of building samples that are actually free of building damage and predicted as undamaged by the model, that is, the number of correctly identified normal power supply areas; the false negatives are the total number of samples that are actually free of building damage but misclassified as minor damage, severe damage or complete destruction, corresponding to the misjudgment of normal power supply areas as having power outage risks; the false positives are the total number of samples that actually have different degrees of building damage but misclassified as undamaged, corresponding to the missed judgment of areas with power outage risks as normal power supply areas.

Figure 13 depicts the four-class confusion matrix of ResiDS-Net on the fine-grained building damage grading task, with rows corresponding to true labels and columns to predicted labels. The no damage class achieves perfect classification with all 200 samples correctly identified, showing the model's strong ability to distinguish intact buildings from damaged ones. For the two high-risk grades closely related to outage risk, namely, major damage and destruction, the numbers of correctly classified samples reach 197 and 184, respectively, and most misclassifications only occur between adjacent damage grades with no severe cross-grade misjudgment. This indicates that the model can reliably identify buildings with structural damage that may cause power outages, providing a solid basis for secondary outage risk judgment. The main classification errors lie in the minor damage grade; 17 samples are mispredicted as major damage and 17 as destruction. Such confusion arises from ambiguous visual features between minor non-structural damage and early-stage structural damage, which is a common challenge in fine-grained disaster image interpretation. On the whole, the model maintains high recognition precision for the critical damage grades dominating outage risk, which effectively guarantees the accuracy of the second-stage fine judgment in the two-stage perception framework.

The ROC curve in Figure 14 is drawn based on the fine-grained damage grading results of individual buildings using the One-vs-Rest strategy, with the false positive rate as the horizontal axis and the true positive rate as the vertical axis, and the blue dashed line passing through the origin represents the random guess curve. The larger the area under the curve and the farther it lies above the random guess line, the better the model's discrimination performance for that category, the result of which determines the accuracy of the secondary judgment of regional power outage risk status. ResiDS-Net exhibits excellent classification performance across all four damage levels: the AUC of the no damage category reaches 0.9999, that of severe damage is 0.9979, and that of complete destruction is 0.9929, all of which are close to 1.0, indicating that the model has strong discriminative ability for intact, severely damaged, and completely collapsed buildings. The AUC of the minor damage category is 0.9865, which, although slightly lower than the other three categories, still maintains high classification accuracy, owing to the blurred visual feature boundaries for judging damage severity, an inherent difficulty of this task.

Severe damage and complete destruction are two critical building damage levels for the secondary judgment of regional outage risk. Only when these two types of buildings exist in an area will it be finally determined as a high-power-outage-risk area. The AUC values of ResiDS-Net for these two categories reach as high as 0.9979 and 0.9929, respectively, which ensure that the model can accurately identify severely damaged and completely destroyed buildings that are crucial for power outage judgment, thus reducing missed detections and false detections in the secondary judgment process.

4.3. Discussion

Aiming at the problem of power outage risk perception for medium- and low-voltage distribution networks in complex scenarios after typhoon disasters, this study proposes the ResiDS-Net method for distribution network power outage risk perception, which identifies power outage risk regions by recognizing satellite images of buildings with different damage levels after typhoons. The ResiDS-Net proposed in this study adopts the improved Dempster–Shafer evidence theory to fuse the decision results of CM-ResNet50, Inception-V3 and DenseNet121, which can effectively improve the perception accuracy of power outage risk regions.

In this study, all networks were trained and tested. The test results show that the proposed ResiDS-Net model achieves an accuracy 2.13% higher than the second-best network in the task of preliminary power outage risk perception for building damage after typhoon disasters, and an accuracy 2.50% higher than the second-best network in the task of graded damage and power outage risk perception for buildings after typhoon disasters. The batch sizes of the networks in the two power outage risk perception tasks were set to 64, 128 and 256, respectively, and training was carried out with learning rates ranging from 0.0001 to 0.0005. The training and test performance of the ResiDS-Net model shows no obvious difference from the results presented above. It can therefore be concluded that the ResiDS-Net model is insensitive to variations in the set batch size and learning rate.

When the RMSP optimizer and SGDM optimizer are adopted, the test results of each network for the preliminary power outage risk perception task of building damage after typhoon disasters are shown in Tables 9 and 10, respectively. It can be concluded from the results in Tables 9 and 10 that the training and test performance of ResiDS-Net with the Adam optimizer is superior to that with the RMSP optimizer and SGDM optimizer. When using the RMSP optimizer and SGDM optimizer, the CM-ResNet50 network proposed in this study performs best among networks with a training time within 3000 s, achieving accuracies of 94.26% and 90.12%, respectively. The ResiDS-Net proposed in this study can achieve the best performance among all 10 networks, with accuracies of 96.13% and 93.46%, respectively. The bolded sections in Tables 9 and 10 are intended to better illustrate the performance of the proposed ResiDS-Net method.

To validate the effectiveness of each component in ResiDS-Net, this study conducts ablation experiments and statistical significance tests. To independently evaluate the contribution of each module, the following comparative configurations are established: ResNet50 is compared with CM-ResNet50 to verify the standalone effect of the Conv Modulation module; the best single branch DenseNet121 (without CM-ResNet50) is compared with simple averaging to verify whether a simple multi-model ensemble already improves performance; and simple averaging and majority voting are compared with the proposed DS fusion to verify the advantage of the improved DS evidence theory over naive ensemble methods. The results of the ablation experiments are shown in Table 11.

Table 9. Training and test results with the RMSP optimizer.

Name	F1 Score (%)	Precision (%)	Test Accuracy (%)	Train Time (s)
ResiDS-Net	**94.83**	**96.38**	**96.13**	**3368.11**
CM-ResNet50	92.36	93.53	94.26	2358.36
ResNet50	90.94	92.09	93.19	2311.81
DenseNet121	90.65	92.99	93.06	2331.29
Inception-V3	90.60	88.33	92.66	3368.09
VGG16	91.48	90.69	93.46	3547.86
VGG19	90.35	93.94	92.92	3849.72
ConvNeXt	92.98	92.98	94.66	3756.92
ResNet101	91.04	91.20	93.19	2508.76
GhostNet-V2	49.68	64.61	68.89	3018.83

Table 10. Training and test results with the SGDM optimizer.

Name	F1 Score (%)	Precision (%)	Test Accuracy (%)	Train Time (s)
ResiDS-Net	**91.51**	**90.41**	**93.46**	**2761.47**
CM-ResNet50	87.54	84.14	90.12	2401.87
ResNet50	86.23	87.96	89.72	2302.29
DenseNet121	86.69	84.39	89.59	2338.77
Inception-V3	86.28	88.85	89.85	2761.45
VGG16	42.61	74.56	69.43	2703.42
VGG19	89.29	90.91	91.99	3798.13
ConvNeXt	20.59	63.64	63.95	2661.59
ResNet101	87.11	90.23	90.52	3066.35
GhostNet-V2	47.25	56.39	61.95	2355.20

Table 11. Ablation test results.

Configuration	F1 Score (%) for Dataset 1	F1 Score (%) for Dataset 2	Test Accuracy (%) for Dataset 1	Test Accuracy (%) for Dataset 2
ResNet50	90.57	88.38	92.66	88.38
CM-ResNet50	92.17	90.34	93.99	90.50
DenseNet121	92.74	88.93	94.53	89.12
Simple average of three branches	90.12	89.72	92.39	89.88
Majority vote	89.74	88.33	92.12	88.50
ResiDS-Net	**95.57**	**92.89**	**96.66**	**93.00**

In the ablation experiments, this study refers to the "post-typhoon building damage and power outage risk perception" dataset as Dataset 1, and the "post-typhoon building graded damage and power outage risk perception" dataset as Dataset 2. The bolded sections in Table 11 are intended to better illustrate the performance of the proposed ResiDS-Net method.

The ablation experiment results show the following: (1) The Conv Modulation (CM) module increased the accuracy of ResNet50 by 1.33% and 2.12% on the two datasets, respectively, confirming its effectiveness in enhancing the focus on deep-layer damaged features. (2) The accuracy of simple averaging did not significantly outperform that of the optimal single-branch DenseNet121 without CM-ResNet50, and even showed a slight decline, indicating that multi-model ensembles are not necessarily beneficial for this task. (3) The DS fusion proposed in this paper further outperforms simple averaging and majority voting. Compared to simple averaging, DS fusion improved accuracy by 4.27% and 3.12% on the two datasets, respectively, validating the advantages of the improved DS evidence theory over naive ensemble methods.

To verify the statistical significance of the performance improvements achieved by ResiDS-Net, this study conducted non-parametric Bootstrap analyses on all comparison models across two datasets, as presented in Tables 12 and 13. Bootstrap is a resampling method that estimates the distribution of a statistic by repeatedly drawing samples with replacement, requiring no prior assumptions about the data distribution, and is therefore well-suited for the interval estimation of classification accuracy. Specifically, on each dataset, samples of the same size as the original test set were randomly drawn with replacement from the test set. This process was repeated 10,000 times, and the accuracy of each model was computed on each resampled subset, thereby yielding an empirical distribution of accuracies. Based on this distribution, the mean accuracy (Bootstrap mean), standard deviation (Bootstrap standard deviation), and 95% confidence interval (using the 2.5th and 97.5th percentiles) were calculated for each model. The Bootstrap mean reflects the average performance of the model across the resampling process and, together with the original test accuracy, validates the stability of the results. The Bootstrap standard deviation measures the degree of variability in accuracy attributable to sampling fluctuations in the test set. The 95% confidence interval quantifies, from a statistical inference perspective, the plausible range of the model's true generalization performance. If the confidence intervals of two models do not overlap, their performance difference can be considered statistically significant at the 95% confidence level.

Table 12. Table of Bootstrap statistical analysis results for each model using Dataset 1.

Name	Test Accuracy (%)	95% Confidence Interval (%) (%)	Bootstrap Mean (%)	Bootstrap Standard Deviation (%)
ResiDS-Net	**96.66**	**[95.19%, 97.73%]**	**96.67**	**0.66**
CM-ResNet50	94.26	[92.26%, 95.59%]	93.99	0.86
ResNet50	93.19	[90.79%, 94.39%]	92.67	0.95
DenseNet121	93.06	[92.19%, 95.12%]	94.53	0.89
Inception-V3	92.66	[91.45%, 95.06%]	93.33	0.91
VGG16	93.46	[90.52%, 94.25%]	92.40	0.96
VGG19	92.92	[90.39%, 94.26%]	92.39	0.96
ConvNeXt	94.66	[93.19%, 95.16%]	93.46	0.87
ResNet101	93.19	[92.38%, 94.92%]	94.13	0.85
GhostNet-V2	68.89	[65.82%, 72.49%]	69.17	1.70

Table 13. Table of Bootstrap statistical analysis results for each model on Dataset 2.

Name	Test Accuracy (%)	95% Confidence Interval (%) (%)	Bootstrap Mean (%)	Bootstrap Standard Deviation (%)
ResiDS-Net	**93.00**	**[91.12%, 94.75%]**	**93.00**	**0.90**
CM-ResNet50	90.50	[88.35%, 91.50%]	90.50	1.04
ResNet50	88.38	[85.00%, 89.50%]	88.36	1.14
DenseNet121	89.12	[86.87%, 90.05%]	89.12	1.10
Inception-V3	88.50	[85.55%, 90.05%]	88.51	1.14
VGG16	87.25	[84.88%, 89.50%]	87.26	1.19
VGG19	87.62	[85.38%, 89.88%]	87.64	1.17
ConvNeXt	58.25	[54.75%, 61.63%]	58.23	1.75
ResNet101	89.25	[86.12%, 90.37%]	89.25	1.10
GhostNet-V2	58.00	[54.63%, 61.38%]	58.02	1.74

In the Bootstrap statistical analysis experiments, this study refers to the "post-typhoon building damage and power outage risk perception" dataset as Dataset 1, and the "post-typhoon building graded damage and power outage risk perception" dataset as Dataset 2. The bolded sections in Tables 12 and 13 are intended to better illustrate the performance of the proposed ResiDS-Net method.

On both datasets, ResiDS-Net achieved the highest test accuracy, at 96.66% and 93.00%, respectively, with Bootstrap means of 96.67% and 93.00%, respectively—highly consistent with the original results. Furthermore, its standard deviations were smaller than those of other comparison networks, at 0.66% and 0.90%, respectively, indicating that the ResiDS-Net model's performance is less affected by the randomness of test set sampling, and that the results exhibit good stability.

The 95% confidence intervals were [95.19%, 97.73%] and [91.12%, 94.75%], respectively. The narrow width of these intervals indicates a high precision in estimating the true generalization capability. The confidence intervals for all comparison models are generally at a lower level, with the upper bounds of most models falling below the lower bound of ResiDS-Net, clearly validating its statistically significant advantage at the 95% confidence level. Even when compared with some advanced models that exhibit similar performance, the numerical values and confidence interval centers of ResiDS-Net remain significantly higher, fully emphasizing the superiority of the proposed method in feature extraction and generalization ability, and demonstrating its effectiveness in practical applications.

From an engineering perspective, the performance gains of ResiDS-Net are cost-effective relative to its increased complexity. The 2.13% and 2.50% accuracy improvements on the two datasets correspond to approximately 16 and 20 additional correctly classified samples, respectively, which directly supports the priority scheduling of emergency repair teams and reduces on-site investigation costs. Computationally, the fully parallel architecture ensures that ResiDS-Net training time (2963.79 s for the coarse screening task) is nearly identical to that of its slowest single sub-network, with no linear time increase. The improved DS fusion is a lightweight post-processing step that adds only sub-millisecond inference latency, keeping single-image inference within 2.02 ms—well within near-real-time requirements for emergency response. Overall, the accuracy gains of the three-branch fusion architecture far outweigh the marginal increase in complexity and computational cost.

In summary, the limitations of this study can be summarized as follows:

1. The ResiDS-Net model requires a large amount of training data, and when image data are insufficient, its classification accuracy and outage risk perception precision decline accordingly;
2. Although the parallel architecture achieves high accuracy, the three-branch feature extraction design still entails considerable training time;
3. The satellite remote sensing-based power outage risk perception method is susceptible to weather conditions such as cloud cover, which may lead to missed detections of outage risk areas;
4. The proposed method is currently only applicable to the power outage risk perception of medium- and low-voltage distribution networks under typhoon disasters, and cannot be directly transferred to other disaster scenarios with distinct power failure mechanisms;
5. Taking building damage as a proxy indicator for distribution network outages has inherent deviations, since the inference is based on the engineering assumption that medium- and low-voltage distribution networks are highly spatially coupled with buildings;
6. The cross-regional generalization performance of the model needs further validation. Tile-level random splitting may implicitly overestimate the model's generalization capability on completely unseen regions.

https://doi.org/10.3390/en19143313

5. Conclusions

This study proposes a power outage risk perception method, which estimates outage risk levels through building damage features extracted from satellite imagery. It is important to clarify that the method provides proxy-based risk inference for post-disaster emergency response, not the ground-truth verification of actual power outage events. To address the difficulties in rapidly and accurately perceiving power outage risk areas of distribution networks after typhoon disasters, as well as the insufficient judgment accuracy caused by traditional methods that equate building cluster damage directly to distribution network power outages, this paper proposes the ResiDS-Net power outage risk perception method, which solves the problems of the rapid delineation and precise assessment of large-scale suspected outage-risk areas. The ResiDS-Net method infers the outage risk level of distribution networks by identifying the degree of building damage, and fuses the decision outputs of three networks, namely, CM-ResNet50, Inception-V3 and DenseNet121, using an improved Dempster–Shafer evidence theory. Meanwhile, a two-stage perception architecture with a "coarse screening–fine judgment" dual-dataset structure is constructed. The suspected power outage range is first quickly delineated using the building cluster damage dataset, and then the damage level of individual buildings is classified with the building graded damage dataset, so as to realize the precise assessment of outage risk levels. The experimental results show that ResiDS-Net achieves an accuracy of 96.66% on the building cluster damage power outage risk perception dataset and 93.00% on the building graded damage power outage risk perception dataset, which are 2.13% and 2.50% higher than those of the nine comparison networks including Inception-V3, respectively. Within the scope of the adopted experimental datasets, the proposed method can effectively improve the accuracy of building-damage-based outage risk perception for distribution networks after typhoon disasters, and provides a technical reference for post-disaster power emergency response. The work of this study can be summarized as follows:

1. This study proposes ResiDS-Net with a parallel network structure, which can extract vital feature information at different scales through three subnetworks, reduce feature loss, and alleviate the performance degradation caused by the deepening of layers in traditional serial networks;
2. Compared with existing single deep learning networks, the proposed ResiDS-Net effectively integrates the respective advantages of CM-ResNet50, Inception-V3 and DenseNet121 via the improved Dempster–Shafer evidence theory, which can improve the prediction accuracy of power outage risk areas in distribution networks;
3. Aiming at the shortcomings of traditional DS evidence theory in multi-source decision fusion, such as noise sensitivity, equal weighting, and decision paradoxes easily induced by evidence conflicts, this study presents an improved DS method. By modifying belief assignment, adapting adaptive evidence weighting, optimizing conflict resolution rules and adding decision probability transformation, the adaptability to the multi-source heterogeneous data of distribution networks is enhanced;
4. Compared with the original ResNet50, this study proposes a Conv Modulation module and applies it to CM-ResNet50. By stabilizing feature distribution, capturing global context and implementing dual-branch feature self-modulation, the model's ability to focus on deep damage features and robustness to remote sensing noise are strengthened, making up for the defects of traditional ResNet50, including sensitivity to cloud and fog interference and insufficient fine-grained feature representation.

In future works, we must approach the following issues: (i) To address the issue that training the ResiDS-Net model relies on a large amount of training data, future research will explore the use of transfer learning techniques, enabling the ResiDS-Net model to quickly adapt to complex scenarios with limited samples in power outage risk perception tasks in different regions after typhoon disasters. (ii) To solve the problem that the judgment of power outage risk areas using remote sensing images is affected by weather and cloud cover, a multimodal network perception method combining UAV aerial images and transmission tower video will be proposed in future work. (iii) To mitigate the inherent deviation caused by taking building damage as a proxy for distribution network outages, future work will carry out field investigations of actual power outage events and collect grid operation and maintenance records to establish a quantitative mapping relationship between building damage levels and real outage states. The risk judgment model will be further calibrated with ground truth data, so as to reduce misjudgments caused by proxy indicators and improve the reliability of perception results. (iv) To further verify the out-of-distribution generalization capability of the model and enrich the connotation of multi-source data fusion, future research will carry out strict event-wise and region-wise cross-validation experiments on the basis of the existing tile-level random splitting paradigm, expand the dataset with more cross-regional and multi-hazard samples, and integrate grid-side and environmental information including feeder topology, pole locations, vegetation coverage and terrain features into the perception framework, so as to enhance the engineering applicability of the proposed method in complex scenarios.

Author Contributions: Conceptualization, Y.Z. and J.B.; methodology, X.S.; software, Y.L. (Yang Luo); validation, Y.M. and Y.L. (Yang Luo); formal analysis, X.X. and M.B.; investigation, H.Z.; resources, M.B.; writing—original draft preparation, Y.L. (Yongtu Li); writing—review and editing, P.G.; visualization, L.Y. All authors have read and agreed to the published version of the manuscript.

Funding: This work was supported by Guangxi Power Grid Co., Ltd. under the Business Support Category Grant No. GXKJXM20240262.

Data Availability Statement: The source code and model implementation details supporting the findings of this study are openly available in the GitHub repository at https://github.com/li318411/ResiDS-Net, version v1.00 (accessed on 26 June 2026). The pre-trained model weights are not included due to their large file size (approximately 9.8 GB) but are available from the corresponding author upon reasonable request. The original remote sensing images are derived from the public xBD dataset and are subject to its licensing terms.

Acknowledgments: The authors declare that this study received funding from Guangxi Power Grid Co., Ltd. under the Business Support Category Grant No. GXKJXM20240262. The funder had the following involvement with the study: the affiliated authors participated in data collection, provided operational insights and domain expertise related to distribution network management, and contributed to the conceptualization and investigation of the research. The funder was not involved in the study design.

Conflicts of Interest: Authors Yu Zou, Juan Bai, Xiaonan Shen, Yang Luo, Yiran Mo, Xingtong Xie, Honghui Zhang, and Mingzhi Bin were employed by Guangxi Power Grid Co., Ltd. The remaining authors declare that the research was conducted in the absence of any commercial or financial relationships that could be construed as a potential conflict of interest.

References

1. Hou, Y.; Guo, Q.; Tu, C.; Xiao, F.; Wang, L.; Jiang, F.; Yu, K.; Wang, X. A Review of Single-Phase-to-Ground Fault Regulation Devices for Distribution Networks. *Renew. Sustain. Energy Rev.* **2024**, *200*, 114602. [CrossRef]
2. Li, Y.; Ma, L.; Zhai, C.; Akiyama, M.; Qin, H. A Probabilistic Framework for Assessing and Enhancing the Resilience of Power Systems to Typhoon Hazards. *Reliab. Eng. Syst. Saf.* **2026**, *265*, 111607. [CrossRef]
3. Zhu, J.; Li, B.; Yan, Q.; Su, S.; Yang, H.; Johnston, A.J. Regional Partition Based Rapid Prediction of Power Outages in Distributed Systems Following Flooding. *Results Eng.* **2025**, *27*, 106791. [CrossRef]
4. Cerrai, D.; Watson, P.; Anagnostou, E.N. Assessing the Effects of a Vegetation Management Standard on Distribution Grid Outage Rates. *Electr. Power Syst. Res.* **2019**, *175*, 105909. [CrossRef]

5. Xiang, M.; Min, J.; Wang, Z.; Gao, P. A Novel Fault Early Warning Model Based on Fault Gene Table for Smart Distribution Grids. *Energies* **2017**, *10*, 1963. [CrossRef]
6. Shao, X.; Wang, Z.; Yang, Y.; Zheng, S.; Mu, J. Target Detection in Ship Remote Sensing Images Considering Cloud and Fog Occlusion. *J. Mar. Sci. Eng.* **2026**, *14*, 124. [CrossRef]
7. Xia, Y.; Li, Z.; Xi, Y.; Wu, G.; Peng, W.; Mu, L. Accurate Fault Location Method for Multiple Faults in Transmission Networks Using Travelling Waves. *IEEE Trans. Ind. Informat.* **2024**, *20*, 8717–8728. [CrossRef]
8. Samudrala, A.N.; Amini, M.H.; Kar, S.; Blum, R.S. Distributed Outage Detection in Power Distribution Networks. *IEEE Trans. Smart Grid* **2020**, *11*, 5124–5137. [CrossRef]
9. Xiao, C.; Liao, Y.; Weng, Y. Distribution Grid Line Outage Identification with Unknown Pattern and Performance Guarantee. *IEEE Trans. Power Syst.* **2024**, *39*, 3987–3999. [CrossRef]
10. Najafi Tari, A.; Sepasian, M.S.; Tourandaz Kenari, M. Resilience Assessment and Improvement of Distribution Networks against Extreme Weather Events. *Int. J. Electr. Power Energy Syst.* **2021**, *125*, 106414. [CrossRef]
11. Zhao, Z.; Wang, F.; Chen, S.; Wang, H.; Cheng, G. Deep Object Segmentation and Classification Networks for Building Damage Detection Using the xBD Dataset. *Int. J. Digit. Earth* **2024**, *17*, 2302577. [CrossRef]
12. Habeeb, Z.Q.; Alzaydi, E.Q. Modified Resnet Model for Medical Image-Based Lung Cancer Detection. *Image Vis. Comput.* **2024**, 105752. [CrossRef]
13. Lou, W.; Zhang, D. Applications of Deep Learning in Mineral Discrimination: A Case Study of Quartz, Biotite and K-Feldspar from Granite. *J. Earth Sci.* **2025**, *36*, 29–45. [CrossRef]
14. Talukder, M.d.A. An Improved XAI-Based DenseNet Model for Breast Cancer Detection Using Reconstruction and Fine-Tuning. *Results Eng.* **2025**, *26*, 104802. [CrossRef]
15. Fan, N.; Liu, J.; Ye, L.; Pan, Z.; Dai, Y.; Fan, W. Dempster–Shafer Evidence Theory Based IFA Detection Approach towards Mixed Attacks in VNDN. *Comput. Ind. Eng.* **2025**, *204*, 111084. [CrossRef]
16. Artemchuk, V.; Garbuz, I.; Jamil Alsayaydeh, J.A.; Shkarupylo, V.; Oliinyk, A.; Bin Yusof, M.F.; Herawan, S.G. Unified Resilience Model Using Deep Learning for Assessing Power System Performance. *Heliyon* **2025**, *11*, e42802. [CrossRef] [PubMed]
17. Jacob, R.A.; Paul, S.; Chowdhury, S.; Gel, Y.R.; Zhang, J. Real-Time Outage Management in Active Distribution Networks Using Reinforcement Learning over Graphs. *Nat. Commun.* **2024**, *15*, 4766. [CrossRef] [PubMed]
18. Braik, A.M.; Koliou, M. Automated Building Damage Assessment and Large-Scale Mapping by Integrating Satellite Imagery, GIS, and Deep Learning. *Comput.-Aided Civ. Infrastruct. Eng.* **2024**, *39*, 2389–2404. [CrossRef]
19. Bohlol, P.; Hosseinpour, S.; Soltani Firouz, M. Improved Food Recognition Using a Refined ResNet50 Architecture with Improved Fully Connected Layers. *Curr. Res. Food Sci.* **2025**, *10*, 101005. [CrossRef] [PubMed]
20. Ritzy, R.; Umadevi, V.A.; Girija, K.; Rajan, R. Binary-Class Concrete Surface Crack Detection Using a Transfer Learning Model. *Knowl.-Based Syst.* **2025**, *324*, 113953. [CrossRef]
21. Genç, İ.Y.; Gürfidan, R.; Yiğit, T. Quality Prediction of Seabream Sparus Aurata by Deep Learning Algorithms and Explainable Artificial Intelligence. *Food Chem.* **2025**, *474*, 143150. [CrossRef] [PubMed]
22. Sasidevi, J.; Sathish, A.; Vatchala, S.; Nallusamy, M. NASNet with African Vulture Optimization for Detecting Diabetic Retinopathy Stages in Retinal Fundus Images. *Expert Syst. Appl.* **2026**, *296*, 128910. [CrossRef]
23. Yao, H.; Liu, T.; Li, G.; Qin, C. Screen-Shot and Demoiréd Image Identification Based on DenseNet and DeepViT. *Expert Syst. Appl.* **2024**, *240*, 122580. [CrossRef]
24. Diykh, M.; Ali, M.; Jamei, M.; Abdulla, S.; Uddin, M.P.; Farooque, A.A.; Labban, A.H.; Alabdally, H. Empirical Curvelet Transform Based Deep DenseNet Model to Predict NDVI Using RGB Drone Imagery Data. *Comput. Electron. Agric.* **2024**, *221*, 108964. [CrossRef]
25. Roy, A.M.; Bhaduri, J. DenseSPH-YOLOv5: An Automated Damage Detection Model Based on DenseNet and Swin-Transformer Prediction Head-Enabled YOLOv5 with Attention Mechanism. *Adv. Eng. Inf.* **2023**, *56*, 102007. [CrossRef]
26. Ji, J.; Feng, Z.; Chen, S. Enhanced Prediction of Partial Nitrification-Anammox Process in Wastewater Treatment by Developing an Attention-Based Deep Learning Network. *J. Environ. Manag.* **2025**, *374*, 124012. [CrossRef] [PubMed]
27. Zhao, L.; Kang, S.; Yoon, S.; Li, J.; Wang, P. Fault Diagnosis Method for Data Imbalance in Chiller Systems Based on CWGAN-GP and DS Evidence Theory Fusion. *Build. Environ.* **2025**, *282*, 113271. [CrossRef]
28. Zhang, H.; Chang, Y.; Zhang, Y.; Kang, B. Evaluate the Competence of Fuzzy Preference Using Statistical Conflict in the Frame of DS Evidence Theory. *Appl. Soft Comput.* **2024**, *164*, 112017. [CrossRef]
29. Li, Y.; Shao, X. Multi-Source Domain Adaptation with Knowledge Transfer for Credit Risk Classification. *Eng. Appl. Artif. Intell.* **2026**, *166*, 113656. [CrossRef]
30. Lei, Z.; Zhang, Z.; Zhou, B.; Chen, H.; Dou, G.; Wang, Y. Transient Interference Suppression Method Based on an Improved TK Energy Operator and Fuzzy Reasoning. *IEEE Trans. Geosci. Remote Sens.* **2023**, *61*, 1–14. [CrossRef]
31. Wu, L.; Liu, Y.; Zhang, J.; Zhang, B.; Wang, Z.; Tong, J.; Li, M.; Zhang, A. Identification of Flood Depth Levels in Urban Waterlogging Disaster Caused by Rainstorm Using a CBAM-Improved ResNet50. *Expert Syst. Appl.* **2024**, *255*, 124382. [CrossRef]

32. Zhu, H.; Wang, W.; Ulidowski, I.; Zhou, Q.; Wang, S.; Chen, H.; Zhang, Y. MEEDNets: Medical Image Classification via Ensemble Bio-Inspired Evolutionary DenseNets. *Knowl.-Based Syst.* **2023**, *280*, 111035. [CrossRef]
33. İncir, R.; Bozkurt, F. Improving Brain Tumor Classification with Combined Convolutional Neural Networks and Transfer Learning. *Knowl.-Based Syst.* **2024**, *299*, 111981. [CrossRef]
34. Guntreddi, V.; Sivakumar, V. Deep Learning Based Glaucoma Detection Using Majority Voting Ensemble of ResNet50, VGG16, and Swin Transformer. *Results Eng.* **2025**, *28*, 107229. [CrossRef]
35. Windriasari, I.; Rahmatulloh, A. Vision-Enhanced Classification and Interpretability for Solar Panel Defect Renewable Energy Using Modified Visual Geometry Group 19. *Eng. Appl. Artif. Intell.* **2026**, *176*, 114808. [CrossRef]
36. Guo, B.; Qiao, Z.; Zhang, N.; Wang, Y.; Wu, F.; Peng, Q. Attention-Based ConvNeXt with a Parallel Multiscale Dilated Convolution Residual Module for Fault Diagnosis of Rotating Machinery. *Expert Syst. Appl.* **2024**, *249*, 123764. [CrossRef]
37. Ren, S.; Chen, B.; Dhupia, J.S.; Stommel, M.; Xu, W. Analyzing Food Bolus Formation during Chewing through Image Segmentation. *Eng. Appl. Artif. Intell.* **2025**, *160*, 111884. [CrossRef]
38. Lu, Q.; Ju, W.; Yin, L. Parallel GhostNet Classification Prediction Method for Supercapacitor Remaining Useful Life Prediction. *Adv. Eng. Inf.* **2024**, *62*, 102916. [CrossRef]